

# A SAINT-VENANT MODEL FOR OVERLAND FLOWS WITH PRECIPITATION AND RECHARGE

MEHMET ERSOY, OMAR LAKKIS, AND PHILIP TOWNSEND

ABSTRACT. We propose a one-dimensional Saint-Venant (open channel) model overland flows including a water input–output source term modelling recharge via rainfall and infiltration (or exfiltration). We derive the model via asymptotic reduction from the two-dimensional Navier–Stokes equations under the shallow water assumption, with boundary conditions including recharge via ground infiltration and runoff. This new model recovers existing models as special cases, and adds more scope by adding a water-mixing friction terms that depends on the rate of water recharge. We propose a novel entropy function and its flux, that are useful in validating the model’s conservation or dissipation properties. Based on this entropy function we propose a finite volume scheme extending a class of kinetic schemes and provide numerical comparisons with respect to the newly introduced mixing friction coefficient. We also provide a comparison with experimental data.

## 1. INTRODUCTION

In quantifying the dynamics of a watercourse, the most important component of the hydrologic recharge and loss is the the *precipitation* and *infiltration* processes, respectively. This is particularly important today in understanding and forecasting the impact of climate variability on the human and natural environment. Modelling these processes and predicting the motion of water is a difficult task to which substantial effort has been devoted [Grace and Eagleson, 1966, Woolhiser and Liggett, 1967, Zhang and Cundy, 1989, Esteves et al., 2000, Weill et al., 2009, Rousseau et al., 2012].

One of the most widely used models to describe the overland motion of watercourses is the classical *one-dimensional Saint-Venant system* (also known as the *open channel* or *shallow water equations*) developed by Adh mar Jean Claude Barr  de Saint-Venant in the 19th Century as a reduction of the Navier–Stokes equation under certain assumptions on the horizontal and vertical scales [de Saint-Venant, 1871]. For the specific problem of modelling flooding caused by precipitation, the inclusion of a source term corresponding to the recharge or infiltration in the Saint-Venant system turns it from a conservation law into a balance law. Existing approaches modelling surface flows under the effect of rainfall or runoff are provided, for example, by Sochala [2008] and Delestre et al. [2012], who model this phenomenon using the system

$$\begin{aligned} \partial_t h + \partial_x [hu] &= S \\ \partial_t [hu] + \partial_x \left[ hu^2 + \frac{g h^2}{2} \right] &= -g h \partial_x Z - k_0(u)u \end{aligned} \tag{1.1}$$

where the unknowns  $h(t, x)$  and  $u(t, x)$  model, respectively, the *height* and *velocity of the water column* at space-time point  $(t, x)$ ,  $g$  the gravitational acceleration (considered a constant  $\approx 9.81m/s^2$ ),  $Z(x)$  the topography of the channel bed with slope  $\partial_x Z(x)$ , and  $k_0$  an empirical fluid-wall friction. The *source term*  $S$  quantifies the amount of water that is added to ( $S > 0$ ) or subtracted from ( $S < 0$ ) from the flow, which in practice may occur through a variety of mechanisms, (e.g. direct rainfall, lateral flow, run-off, smaller tributaries). Among early works including the effect of rainfall (or lateral inflow) on surface flows that relate to this research, we note Woolhiser and Liggett [1967], Wenzel [1970], and Zhang and Cundy [1989].

Our goal in this paper is to derive a model akin to (1.1) via vertical averaging under the shallow water assumption, starting from the Navier–Stokes equations with a permeable Navier boundary condition to account for the infiltration and a kinematic boundary condition to consider the precipitation. The obtained averaged model extends this system in a unique manner through an additional momentum source term of the form

$$Su - (k_+(R) + k_-(I))u \quad \text{with } S := R - I, \tag{1.2}$$

where  $R \geq 0$  denotes the *recharge rate* on the free surface (accounting for both rain and runoff effects) and  $I$  denotes the *infiltration rate* from the water to the ground (when  $I > 0$ ) or the ground to the water (when  $I < 0$ ), i.e., *seepage*, sometimes called *exfiltration*. The terms  $k_+(R)$  and  $k_-(I)$ , which will be discussed in detail in §2.1, model the friction caused by *recharge*, i.e., the addition of water (assumed to have zero horizontal velocity), which attaches to and is advected by the flow. We will see below that these friction terms are necessary to avoid paradoxical outcomes such as perpetual motion, and, for simplicity, we will assume in this paper the most basic constitutive relations for this friction: linear in  $R$  for  $k_+(R)$  and piecewise linear in  $I$  for  $k_-(I)$ . We note, however, that these terms could be generalised

by having two separate friction coefficients or by replacing the linearity with more precise constitutive relations.

We outline the rest of the article as follows: in §2, we present the geometric setup of the system and the adjusted boundary conditions (including precipitation, infiltration, and the corresponding friction terms) of the typical Navier–Stokes equations. In §3, we derive the consequent Saint-Venant system through a first order approximation and discuss several theoretical results and corollaries that can be derived for the system in §4. In §5, we adapt to our model the finite volume kinetic scheme considered in Audusse et al. [2000] and Perthame and Simeoni [2001], and finally present numerical experiments of the resulting code to demonstrate the application of the model in §6. A C and C++ implementation of this code, written by Matthieu Besson, Omar Lakkis and Philip Townsend, is freely available on request (an older version is given by Besson et al. [2013]).

## 2. NAVIER–STOKES EQUATIONS WITH INFILTRATION AND RECHARGE

Our aim is to construct a mathematical model for overland flows that is consistent with the physical phenomena that can affect the motion of such water. To this purpose, we propose a model reduction of the two-dimensional Navier–Stokes equations leading to an extension of the standard Saint-Venant system. By considering suitably chosen boundary conditions, we take into account the addition and removal of water, either by rainfall (e.g. from runoff onto the top of the watercourse) or by groundwater infiltration or exfiltration processes (e.g via a porous soil).

We start in §2.1 by reviewing the Navier–Stokes equations in the special geometric setting, describing the physics with a *wet boundary* on the bottom of the water course and a *free surface* on the top. We then introduce the boundary conditions for each surface in §2.2 and §2.3, respectively.

### 2.1. Geometric set-up and the two-dimensional Navier–Stokes equations.

With numerical and practical applications in mind, we assume an arbitrary final time  $T > 0$ . With reference to Fig. 1, we consider an incompressible fluid moving in the space-time box

$$[0, T] \times \mathbb{R}^2 \text{ with typical point denoted } (t, x, z). \quad (2.1.1)$$

The *absolute height* of the surface of the watercourse and the *topography* of the channel bed are modelled, respectively, by the functions

$$\begin{aligned} H : [0, T] \times \mathbb{R} &\rightarrow \mathbb{R} & Z : \mathbb{R} &\rightarrow \mathbb{R} \\ (t, x) &\mapsto H(t, x), & x &\mapsto Z(x), \end{aligned} \quad (2.1.2)$$

whose values measure with respect to a *reference horizontal height* 0. We define the *local height* of the water by

$$h(t, x) := H(t, x) - Z(x). \quad (2.1.3)$$

We assume that there exists  $c \in \mathbb{R}$  such that  $\int_{\mathbb{R}} Z(x) - c \, dx$  is finite. This assumption which is not restrictive from a modelling point of view will be necessary for entropy balance considerations. Furthermore the vertical reference axis can be chosen so that  $c = 0$ . The *wet region* is defined as the area in which the fluid resides at each time  $t \in [0, T]$

$$\Omega(t) := \{(x, z) \in \mathbb{R}^2 : Z(x) < z < H(t, x)\}, \quad (2.1.4)$$

with its global counterpart

$$\Omega := \bigcup_{0 \leq t \leq T} \Omega(t). \quad (2.1.5)$$

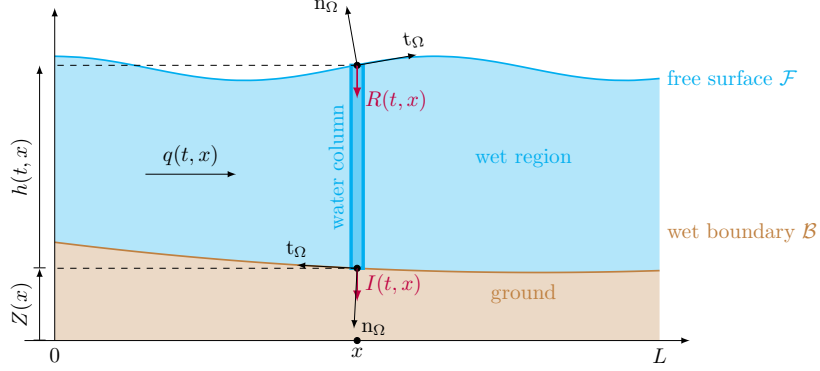


FIGURE 1. Diagram of a river and river bed depicting the variables of interest

As we can see in Figure 1, the wet region has two boundaries; the first is the *wet boundary* between the wet region and the ground, denoted by

$$\mathcal{B} = \{(x, Z) : x \in \mathbb{R}\}, \quad (2.1.6)$$

and the second is the *free surface* between the wet region and the surrounding air, denoted by

$$\mathcal{F} = \{(t, x, H) : t > 0, x \in \mathbb{R}\}. \quad (2.1.7)$$

We assume that the viscous flow  $\mathbf{u}$  satisfies, on the space-time domain  $\Omega$ , the two-dimensional incompressible Navier–Stokes equation

$$\begin{aligned} \operatorname{div} [\rho_0 \mathbf{u}^\top] &= 0, \\ \partial_t [\rho_0 \mathbf{u}] + \operatorname{div} [\rho_0 \mathbf{u} \otimes \mathbf{u}] - \operatorname{div} \boldsymbol{\sigma} [\mathbf{u}] - \rho_0 \mathbf{F} &= 0 \end{aligned} \quad (2.1.8)$$

where  $\mathbf{u} = (u, \mathbf{v})$  is the velocity field,  $\rho_0$  is the density of the fluid (taken to be constant since the fluid is incompressible),  $\mathbf{F} = (0, -g)$  is the external force of gravity with constant  $g$ , and  $\boldsymbol{\sigma} [\mathbf{u}]$  is the total stress tensor whose matrix given by

$$\boldsymbol{\sigma} [\mathbf{u}] := \begin{bmatrix} -p + 2\mu \partial_x u & \mu (\partial_z u + \partial_x \mathbf{v}) \\ \mu (\partial_z u + \partial_x \mathbf{v}) & -p + 2\mu \partial_z \mathbf{v} \end{bmatrix} \quad (2.1.9)$$

where  $p$  is the pressure and  $\mu > 0$  the dynamic viscosity. The (algebraic) tensor product of two vectors  $\mathbf{a} \otimes \mathbf{b}$  is defined as  $\mathbf{a} \mathbf{b}^\top$  (all vectors are displayed as columns) and the  $\operatorname{div}$  of a covector/tensor is taken as the row-wise divergence of the associated matrix; in coordinates this means

$$[\operatorname{div} \boldsymbol{\alpha}]_i = \sum_{j=x,z} \partial_j \alpha_i^j \text{ for } i = x, z \quad (2.1.10)$$

To work with the wet region, we introduce its *indicator function*

$$\Phi(t, x, z) := \mathbb{1}_{\Omega(t)}(x, z) = \mathbb{1}_{[Z(x) \leq z \leq H(t,x)]} \text{ for all } t, x, z \in \mathbb{R}. \quad (2.1.11)$$

The function  $\Phi$  is advected by the flow so its material derivative, with respect to the flow  $\mathbf{u}$ , must therefore be zero. Moreover, thanks to the incompressibility condition,  $\Phi$  satisfies the following *indicator transport equation*

$$\partial_t \Phi + \partial_x [\Phi u] + \partial_z [\Phi \mathbf{v}] = 0 \text{ on } \Omega. \quad (2.1.12)$$

**2.2. The wet boundary.** Crucial to our model derivation is the particular situation on the *wet boundary*, where the effect of *infiltration* plays a central role. Given a set  $G \in \mathbb{R}^2$  and a point  $\mathbf{x} \in \partial G$ , we denote by  $\mathbf{t}_G(\mathbf{x})$  the unique normalized tangential vector and by  $\mathbf{n}_G(\mathbf{x})$  its outward boundary normal (see Fig. 1 for  $G = \Omega$ ).

On the wet boundary, the topography is assumed to be rough and hence produces friction, which we take into account by considering the following *Navier boundary condition*:

$$(\boldsymbol{\sigma}[\mathbf{u}] \mathbf{n}_\Omega) \cdot \mathbf{t}_\Omega = -\rho_0 (k(\mathbf{u}) - k_-(I)) \mathbf{u} \cdot \mathbf{t}_\Omega \quad \text{on } \mathcal{B} \quad (2.2.1)$$

We will leave defining  $k_-(I)$  for the moment and note that the scalar function  $k(\mathbf{u})$  models a general *kinematic friction law* on the channel bed:

$$k(\boldsymbol{\xi}) := (C_{\text{lam}} + C_{\text{tur}} |\boldsymbol{\xi}|), \quad \text{for all } \boldsymbol{\xi} \in \mathbb{R}^2 \quad (2.2.2)$$

where the friction coefficients  $C_{\text{lam}}$  and  $C_{\text{tur}}$  (which by definition are always non-negative) correspond, respectively, to the laminar and turbulent friction factors [Wylie and Streeter, 1978, Streeter et al., 1998, Gerbeau and Perthame, 2001, Levermore and Sammartino, 2001, Marche, 2007]. The ground may also, due to porosity, absorb water (by *infiltration*) or inject water (through *recharge*) from and into the bulk. This mechanism is modelled with the following *permeable boundary condition*:

$$\mathbf{u}(t, x, z) \cdot \mathbf{n}_\Omega(x, z) = I(t, x) \quad \text{on } \mathcal{B}, \quad (2.2.3)$$

where the infiltration function  $I$  models the amount of water that leaves ( $I > 0$ ) or enters ( $I < 0$ ) the flow per elementary boundary element.

The term  $k_-(I)$  models the friction effect that occurs when water that is recharging through the ground (at average microscopic velocity rate zero) connects with the flow. The magnitude of this effect is given by the parameter  $\alpha$ , and hence our *infiltration mixing friction law* is given by

$$k_-(I) := \alpha I_- = \alpha \max(0, -I). \quad (2.2.4)$$

We note that the recharge-induced friction only occurs when water is entering the flow (i.e.  $I < 0$ ), and is zero otherwise. Although  $I$  should in principle be thought of as a function of  $h$ ,  $\mathbf{u}$ , and possibly their derivatives—particularly  $\boldsymbol{\sigma}[\mathbf{u}]$ , as in the recognised Beavers–Joseph–Saffman model described, for instance, by Beavers and Joseph [1967], Saffman [1971], Jäger and Mikelić [2000], Badea et al. [2010]—we ignore this in this paper and for simplicity consider the function  $I$  to be a given piecewise linear function of space-time.

We define  $\Omega$ 's tangential and outward unit normal vectors on  $\mathcal{B}$  by

$$\mathbf{t}_\Omega(x, Z(x)) = \frac{(-1, -\partial_x Z(x))}{\sqrt{1 + |\partial_x Z(x)|^2}} \quad (2.2.5)$$

and

$$\mathbf{n}_\Omega(x, Z(x)) = \frac{(\partial_x Z(x), -1)}{\sqrt{1 + |\partial_x Z(x)|^2}}, \quad (2.2.6)$$

respectively, following the convention that the outward normal is the tangential vector rotated by  $\pi/2$  counterclockwise. It thus follows that (2.2.1) and (2.2.3) on  $\mathcal{B}$  can be rewritten, respectively, as

$$\begin{aligned} & \frac{\mu (\partial_x v + \partial_z u) (1 - |\partial_x Z|^2) - 2\mu (\partial_x u - \partial_z v) \partial_x Z}{(1 + |\partial_x Z|^2)^{1/2}} \\ & = \rho_0 (k(u, v) + k_-(I)) (u + v \partial_x Z) \end{aligned} \quad (2.2.7)$$

and

$$\mathbf{v} - u\partial_x Z(x) + I\sqrt{1 + |\partial_x Z|^2} = 0. \quad (2.2.8)$$

**2.3. The free surface.** On the free surface, we neglect all other meteorological phenomena (such as evaporation) and consider only the addition of water in the form of direct rainfall and runoff. Assuming a *kinematic boundary condition*, we set

$$\mathbf{u} \cdot \mathbf{n}_\Omega = \frac{\partial_t H - R}{\sqrt{1 + |\partial_x H|^2}} \quad \text{on } \mathcal{F}, \quad (2.3.1)$$

where  $R(t, x)$  is the recharge rate due to rainfall. The unit tangential and normal vectors  $\mathbf{t}_\Omega$  and  $\mathbf{n}_\Omega$  to the free surface can be explicitly computed in terms of  $H$  as

$$\mathbf{t}_\Omega(x, H(t, x)) = \frac{(1, \partial_x H(t, x))}{\sqrt{1 + |\partial_x H(t, x)|^2}} \quad (2.3.2)$$

and

$$\mathbf{n}_\Omega(x, H(t, x)) = \frac{(-\partial_x H(t, x), 1)}{\sqrt{1 + |\partial_x H(t, x)|^2}}, \quad (2.3.3)$$

which leads to the following explicit form of (2.3.1):

$$\partial_t H + u\partial_x H - v = R \quad \text{on } \mathcal{F}. \quad (2.3.4)$$

We also assume a stress condition on the free surface, given by

$$(\boldsymbol{\sigma}[\mathbf{u}] \mathbf{n}_\Omega) \cdot \mathbf{t}_\Omega = -\rho_0 k_+(R) \mathbf{u} \cdot \mathbf{t}_\Omega, \quad (2.3.5)$$

where we use the *surface mixing friction* law

$$k_+(R) = \alpha R \quad (2.3.6)$$

which takes into account the frictional effect of the additional entering water's mixing with the flow from various sources (runoff, direct rainfall, small-scale tributaries, for example) with  $\alpha$  again representing the magnitude of this effect (see §3.5 for more on mixing friction and references). Using the tangential and normal vectors as above, this condition becomes

$$\frac{\mu(\partial_x v + \partial_z u) \left(1 - |\partial_x H|^2\right) - 2\mu(\partial_x u - \partial_z v) \partial_x H}{\sqrt{1 + |\partial_x H|^2}} = -\rho_0 k_+(R) (u + v\partial_x H). \quad (2.3.7)$$

### 3. SAINT-VENANT SYSTEM WITH RECHARGE VIA VERTICAL AVERAGING

We now proceed to write the Navier–Stokes equations with adapted boundary conditions in non-dimensional form. Under an assumption on the shallowness of the ratio of the water height to the horizontal domain (represented by a small parameter  $\varepsilon$ ), we formally make an asymptotic expansion of the Navier–Stokes system to the hydrostatic approximation at first order. Finally, we derive the Saint-Venant system through an integration on the water height.

This approach follows one established by Gerbeau and Perthame [2001], also found in Ersoy [2015], which we differ from in the boundary conditions for Navier–Stokes that turn into different source terms in the Saint-Venant's equation. Furthermore, we have to take extra care in how we non-dimensionalise our additional precipitation, infiltration, and friction terms. For simplicity, we will start from the two-dimensional Navier–Stokes equations and obtain the one-dimensional

Saint-Venant's equations, although this procedure can be employed to derive a two-dimensional analogue from the three dimensional Navier–Stokes provided the boundary conditions are modified accordingly.

**3.1. Dimensionless Navier–Stokes equations.** To derive the Saint-Venant model, we assume that the water height is small with respect to the horizontal length of the domain and that vertical variations in velocity are small compared to the horizontal variations. This is achieved by postulating a *small parameter* ratio

$$\varepsilon := \frac{D}{L} = \frac{V}{U} \ll 1, \quad (3.1.1)$$

where  $D, L, V$ , and  $U$  are the *scales* (or *units*) of, respectively, water height, domain length, vertical fluid velocity, and horizontal fluid velocity. As a consequence the time scale  $T$  is such that

$$T = \frac{L}{U} = \frac{D}{V}. \quad (3.1.2)$$

We also choose the pressure scale to be

$$P := \rho_0 U^2. \quad (3.1.3)$$

The rationale for this choice is that we are focusing on the effect of the horizontal forces as mass per horizontal acceleration which has a force scale of

$$F := (DL^{2-1}\rho_0)(UT^{-1}), \quad (3.1.4)$$

and these forces are applied to vertical boundary scale to give the pressure scale

$$F (DL^{2-2})^{-1} = DL\rho_0 UT^{-1} D^{-1} = \rho_0 UL T^{-1} = \rho_0 U^2. \quad (3.1.5)$$

It is convenient to define the spatial characteristic length,  $L$ , and horizontal velocity,  $U$ , (and by definition  $T$ ) as finite constants with respect to  $\varepsilon \rightarrow 0$ , while the water height and vertical velocity are defined as  $D = \varepsilon L$  and  $V = \varepsilon U$ , respectively. This allows us to introduce the dimensionless quantities of time  $\tilde{t}$ , space  $(\tilde{x}, \tilde{z})$ , pressure  $\tilde{p}$ , and velocity field  $(\tilde{u}, \tilde{v})$  via the following scaling relations:

$$\left\{ \begin{array}{l} \tilde{t} := \frac{t}{T}, \quad \tilde{p}(\tilde{x}, \tilde{t}, \tilde{z}) := \frac{p(x, t, z)}{P}, \\ \tilde{x} := \frac{x}{L}, \quad \tilde{u}(\tilde{x}, \tilde{t}, \tilde{z}) := \frac{u(x, t, z)}{U}, \\ \tilde{z} := \frac{z}{D} = \frac{z}{\varepsilon L}, \quad \tilde{v}(\tilde{x}, \tilde{t}, \tilde{z}) := \frac{v(x, t, z)}{V} = \frac{v(x, t, z)}{\varepsilon U} \end{array} \right\}. \quad (3.1.6)$$

We also rescale the laminar and turbulent friction factors as, respectively,

$$C_{\text{lam},0} := \frac{C_{\text{lam}}}{V} = \frac{C_{\text{lam}}}{\varepsilon U}, \quad C_{\text{tur},0} := \frac{C_{\text{tur}}}{\varepsilon}, \quad (3.1.7)$$

and the infiltration and rainfall rates as, respectively,

$$\tilde{I}(\tilde{t}, \tilde{x}) := \frac{I(t, x)}{V}, \quad \tilde{R}(\tilde{t}, \tilde{x}) := \frac{R(t, x)}{V}. \quad (3.1.8)$$

Note that in the assumed asymptotic setting,  $C_{\text{lam},0}$  and  $C_{\text{tur},0}$  are constants with respect to  $\varepsilon$ , thus implying that  $C_{\text{lam}}$  and  $C_{\text{tur}}$  vanish linearly with  $\varepsilon \rightarrow 0$ . Finally, we define the following non-dimensional numbers:

$$\begin{aligned} \text{Froude's number,} & \quad \text{Fro} := U/\sqrt{gD}, \\ \text{Reynolds's number with respect to } \mu, & \quad \text{Rey} := \rho_0 UL/\mu, \end{aligned} \quad (3.1.9)$$

and consider the following asymptotic setting

$$\text{Rey}^{-1} = \varepsilon\mu_0, \quad (3.1.10)$$

where  $\mu_0$  is the *viscosity*.

Using these dimensionless variables in the Navier–Stokes equations (2.1.8) and (2.1.9), and reordering the terms with respect to powers of  $\varepsilon$ , the dimensionless incompressible Navier–Stokes system reads as follows:<sup>1</sup>

$$\begin{aligned} \operatorname{div}[\tilde{\mathbf{u}}] &= 0 \\ \partial_{\tilde{t}}\tilde{u} + \partial_{\tilde{x}}[\tilde{u}^2] + \partial_{\tilde{z}}[\tilde{u}\tilde{v}] + \partial_{\tilde{x}}\tilde{p} &= \partial_{\tilde{z}}\left[\frac{\mu_0}{\varepsilon}\partial_{\tilde{z}}\tilde{u}\right] + \varrho_{3.1.12,\varepsilon,\tilde{\mathbf{u}}} \\ \partial_{\tilde{z}}\tilde{p} &= -\frac{1}{\operatorname{Fro}^2} + \varrho_{3.1.13,\varepsilon,\tilde{\mathbf{u}}} \end{aligned} \quad (3.1.11)$$

where

$$\varrho_{3.1.12,\varepsilon,\tilde{\mathbf{u}}} := \varepsilon\mu_0\left(2\partial_{\tilde{u}}\tilde{x}\tilde{x} + \partial_{\tilde{v}}\tilde{z}\tilde{x}\right) \quad (3.1.12)$$

and

$$\varrho_{3.1.13,\varepsilon,\tilde{\mathbf{u}}} := \varepsilon\mu_0\left(\partial_{\tilde{x}\tilde{z}}\tilde{u} + \varepsilon^2\partial_{\tilde{x}\tilde{x}}\tilde{v} + 2\partial_{\tilde{z}\tilde{z}}\tilde{v}\right) - \varepsilon^2\left(\partial_{\tilde{t}}\tilde{v} + \partial_{\tilde{x}}[\tilde{u}\tilde{v}] + \partial_{\tilde{z}}[\tilde{v}^2]\right). \quad (3.1.13)$$

Assuming  $\tilde{\mathbf{u}}$  has bounded second derivatives, definitions (3.1.12) and (3.1.13) formally lead to

$$\varrho_{3.1.12,\varepsilon,\tilde{\mathbf{u}}} = \mathcal{O}(\varepsilon) \quad \text{and} \quad \varrho_{3.1.13,\varepsilon,\tilde{\mathbf{u}}} = \mathcal{O}(\varepsilon). \quad (3.1.14)$$

On the wet boundary  $\mathcal{B}$ , recalling the scaling relations (3.1.6) and (3.1.8), and noting that

$$\frac{\partial Z}{\partial x} = \frac{\varepsilon L}{L} \frac{\partial \tilde{Z}}{\partial \tilde{x}} = \varepsilon \partial_{\tilde{x}} \tilde{Z}, \quad (3.1.15)$$

the dimensionless Navier boundary condition (2.2.7) implies

$$\begin{aligned} \left[\frac{\partial_{\tilde{z}}\tilde{u}}{\varepsilon\operatorname{Rey}}\right]_{\mathcal{B}} &= \left(\frac{C_{\text{lam}}}{U}\tilde{u} + C_{\text{tur}}(|\tilde{u}| + \varepsilon|\tilde{v}|)\tilde{u} + \varepsilon k_-(\tilde{I})\tilde{u}\right) \frac{\sqrt{1 + \varepsilon^2(\partial_{\tilde{x}}\tilde{Z})^2}}{1 - \varepsilon^2(\partial_{\tilde{x}}\tilde{Z})^2} \\ &\quad + \underbrace{\varepsilon^2\partial_{\tilde{x}}\tilde{Z}\left(\frac{C_{\text{lam}}}{U}\tilde{v} + C_{\text{tur}}(|\tilde{u}| + \varepsilon|\tilde{v}|)\tilde{v} + \varepsilon k_-(\tilde{I})\tilde{v}\right)}_{\mathcal{O}(\varepsilon^2)} \frac{\sqrt{1 + \varepsilon^2(\partial_{\tilde{x}}\tilde{Z})^2}}{1 - \varepsilon^2(\partial_{\tilde{x}}\tilde{Z})^2} \\ &\quad - \underbrace{\frac{\varepsilon}{\operatorname{Rey}}\left(\partial_{\tilde{x}}\tilde{v} + \frac{2\partial_{\tilde{x}}\tilde{Z}(\partial_{\tilde{z}}\tilde{v} - \partial_{\tilde{x}}\tilde{u})}{1 - \varepsilon^2(\partial_{\tilde{x}}\tilde{Z})^2}\right)}_{\mathcal{O}(\varepsilon/\operatorname{Rey})}. \end{aligned} \quad (3.1.16)$$

Applying the non-dimensional friction factors (3.1.7) and recalling (3.1.10), we get

$$\begin{aligned} \left[\frac{\partial_{\tilde{z}}\tilde{u}}{\varepsilon\operatorname{Rey}}\right]_{\mathcal{B}} &= \varepsilon\left(C_{\text{lam},\varepsilon}\tilde{u} + C_{\text{tur},\varepsilon}(|\tilde{u}| + \varepsilon|\tilde{v}|)\tilde{u} + k_-(\tilde{I})\tilde{u}\right) \frac{\sqrt{1 + \varepsilon^2(\partial_{\tilde{x}}\tilde{Z})^2}}{1 - \varepsilon^2(\partial_{\tilde{x}}\tilde{Z})^2} + \mathcal{O}(\varepsilon^2) \\ &= \varepsilon\left(C_{\text{lam},\varepsilon}\tilde{u} + C_{\text{tur},\varepsilon}|\tilde{u}|\tilde{u} + k_-(\tilde{I})\tilde{u}\right) + \mathcal{O}(\varepsilon^2) \\ &= \varepsilon\left(k_0(\tilde{u}) + k_-(\tilde{I})\right)\tilde{u} + \mathcal{O}(\varepsilon^2), \end{aligned} \quad (3.1.17)$$

with *asymptotic friction laws*

$$\begin{aligned} k_0(\xi) &:= C_{\text{lam},0} + C_{\text{tur},0}|\xi| \quad \text{for } \xi \in \mathbb{R} \\ k_-(\tilde{I}) &:= \alpha I_- = -\min(0, \tilde{I}) \quad \text{for } \alpha \in \mathbb{R}, \end{aligned} \quad (3.1.18)$$

<sup>1</sup>We bind all the “tilde” variables together, i.e.,  $\tilde{u}$  is a function of  $\tilde{t}, \tilde{x}, \tilde{z}$ . Hence variableless operators change accordingly, e.g.,  $\operatorname{div}\tilde{\mathbf{u}}$  means  $\operatorname{div}_{(\tilde{x},\tilde{z})}(\tilde{u}, \tilde{v})$  when  $\operatorname{div}\mathbf{u}$  means  $\operatorname{div}_{(x,z)}(u, v)$ .



on the wet boundary. The permeable boundary condition (2.2.8) reads

$$\tilde{v} = \tilde{u}\partial_x Z - I\sqrt{1 + \varepsilon^2(\partial_x Z)^2} = \tilde{u}\partial_x Z - I + O(\varepsilon). \quad (3.1.19)$$

For the boundary conditions on the free surface  $\mathcal{F}$ , applying our non-dimensionalisation approach to the kinematic boundary condition (2.3.4) we derive

$$\partial_t \tilde{H} + u\partial_x \tilde{H} - \tilde{v} = \tilde{R}, \quad (3.1.20)$$

while we can non-dimensionalise (2.3.7) in the same manner as the Navier boundary condition (2.2.7) on the wet boundary  $\mathcal{B}$ , giving

$$\left[ \frac{\partial_z \tilde{u}}{\varepsilon \text{Rey}} \right]_{\mathcal{F}} = -\varepsilon k_+(\tilde{R})\tilde{u} + O(\varepsilon^2), \quad (3.1.21)$$

with free surface asymptotic friction law

$$k_+(\tilde{R}) = \alpha \tilde{R} \text{ for } \alpha \in \mathbb{R}. \quad (3.1.22)$$

**3.2. First order approximation of the dimensionless Navier–Stokes equations.** Dropping all terms of  $O(\varepsilon)$  and above in equations (3.1.11)–(3.1.21), we deduce the hydrostatic approximation of the dimensionless Navier–Stokes system

$$\partial_x u_\varepsilon + \partial_z v_\varepsilon = 0 \quad (3.2.1)$$

$$\partial_t u_\varepsilon + \partial_x [u_\varepsilon^2] + \partial_z [u_\varepsilon v_\varepsilon] + \partial_x p_\varepsilon = \partial_z \left[ \frac{\mu_0}{\varepsilon} \partial_z u_\varepsilon \right] \quad (3.2.2)$$

$$\partial_z p_\varepsilon = -\frac{1}{\text{Fro}^2}, \quad (3.2.3)$$

whilst the boundary conditions, as a result of the asymptotic setting (3.1.10), simplify to

$$\left[ \frac{\mu_0}{\varepsilon} \partial_z u_\varepsilon \right] = (k_0(u_\varepsilon) + k_-(I)) u_\varepsilon \quad \text{and} \quad v_\varepsilon = u_\varepsilon \partial_x Z - I \text{ on } \mathcal{B}, \quad (3.2.4)$$

and

$$\left[ \frac{\mu_0}{\varepsilon} \partial_z u_\varepsilon \right] = -k_+(R) u_\varepsilon \quad \text{and} \quad \partial_t H + u_\varepsilon \partial_x H - v_\varepsilon = R \text{ on } \mathcal{F}, \quad (3.2.5)$$

in view of equations (3.1.17), (3.1.19), (3.1.21), and (3.1.20), respectively. Here,  $(u_\varepsilon, v_\varepsilon, p_\varepsilon)$  represents the solution of the first-order dimensionless Navier–Stokes system.

Vertically integrating both members of equation (3.2.3) over  $[z, H(t, x)]$ , we obtain the hydrostatic pressure

$$p_\varepsilon(t, x, H) - p_\varepsilon(t, x, z) = -\frac{1}{\text{Fro}^2}(H(t, x) - z). \quad (3.2.6)$$

Assuming that the pressure exerted by the rain on the free surface  $p_\varepsilon(t, x, H) = p_c$  for some constant  $p_c \in \mathbb{R}$  (as we neglected all other meteorological phenomena), this becomes

$$p_\varepsilon(t, x, z) = \frac{1}{\text{Fro}^2}(H(t, x) - z) + p_c. \quad (3.2.7)$$

Moreover, identifying terms at order  $1/\varepsilon$  in (3.2.2), (3.2.4), and (3.2.5), we obtain the *motion by slices* decomposition

$$u_\varepsilon(t, x, z) = u_0(t, x) + O(\varepsilon) \quad (3.2.8)$$

for some function  $u_0 = u_0(t, x)$ , as a consequence of

$$\partial_z [\mu_0 \partial_z u_\varepsilon] = O(\varepsilon), \text{ for } z \in (Z(x), H(t, x)) \quad (3.2.9)$$

with

$$[\mu_0 \partial_z u_\varepsilon]_{|z=Z(x)} = O(\varepsilon) \text{ and } [\mu_0 \partial_z u_\varepsilon]_{|z=H(t, x)} = O(\varepsilon). \quad (3.2.10)$$

Noting  $\langle u_\varepsilon(t, x) \rangle$  as the mean speed of the fluid over the section  $[Z(x), H(t, x)]$ ,

$$\langle u_\varepsilon(t, x) \rangle = \frac{1}{h(t, x)} \int_{Z(x)}^{H(t, x)} u_\varepsilon(t, x, z) \, dz, \quad (3.2.11)$$

we are able to use the following approximations and drop the first and higher order terms in  $\varepsilon$ :

$$u_\varepsilon(t, x, z) = \langle u_\varepsilon(t, x) \rangle + O(\varepsilon) \quad \text{and} \quad \langle u_\varepsilon(t, x)^2 \rangle = \langle u_\varepsilon(t, x) \rangle^2 + O(\varepsilon). \quad (3.2.12)$$

**3.3. The Saint-Venant system with recharge.** Keeping in mind (3.2.12) and integrating the indicator transport equation (2.1.12) for  $z \in [Z(x), H(t, x)]$ , we get

$$\begin{aligned} 0 &= \int_{Z(x)}^{H(t, x)} \partial_t \Phi(t, x, z) + \partial_x [\Phi u_\varepsilon] + \partial_z [\Phi v_\varepsilon] \, dz \\ &= \partial_t h + \partial_x q - [\partial_t H + u_\varepsilon \partial_x H - v_\varepsilon]_{z=H(t, x)} + [u_\varepsilon \partial_x Z - v_\varepsilon]_{z=Z(x)}, \end{aligned} \quad (3.3.1)$$

where  $q$  is the discharge defined by

$$q(t, x) := \langle u_\varepsilon(t, x) \rangle h(t, x). \quad (3.3.2)$$

In view of the penetration condition (3.2.4) and the kinematic boundary condition (3.2.5), we deduce the *mass-balance* equation:

$$\partial_t h + \partial_x q = S \quad (3.3.3)$$

where the source term  $S := R - I$  measures the gain or loss of water through the (nonnegative) *recharge rate*  $R$  (ultimately from rainfall) and (signed) *infiltration rate*, respectively.

Keeping equations (3.2.7), (3.2.8), and (3.2.12) in mind and thanks to the penetration condition (3.2.4) and the kinematic boundary condition (3.2.5), integrating the left-hand side of (3.2.2) for  $z \in [Z(x), H(t, x)]$ , we get

$$\begin{aligned} \int_{Z(x)}^{H(t, x)} \text{LHS}(3.2.2) \, dz &= \partial_t q + \partial_x \left[ \frac{q^2}{h} + \frac{h^2}{2\text{Fro}^2} \right] + \frac{h}{\text{Fro}^2} \partial_x Z \\ &\quad - [(\partial_t H + u_\varepsilon \partial_x H - v_\varepsilon) u_\varepsilon]_{(t, x, H(t, x))} \\ &\quad + [(u_\varepsilon \partial_x Z - v_\varepsilon) u_\varepsilon]_{(t, x, Z(x))} \\ &= \partial_t q + \partial_x \left[ \frac{q^2}{h} + \frac{h^2}{2\text{Fro}^2} \right] + \frac{h}{\text{Fro}^2} \partial_x Z \\ &\quad - R [u_\varepsilon]_{(t, x, H(t, x))} + I [u_\varepsilon]_{(t, x, Z(x))} \\ &= \partial_t q + \partial_x \left[ \frac{q^2}{h} + \frac{h^2}{2\text{Fro}^2} \right] + \frac{h}{\text{Fro}^2} \partial_x Z - S \frac{q}{h}, \end{aligned} \quad (3.3.4)$$

where  $S$  is again defined as above. Now, integrating the right-hand side of (3.2.2) for  $z \in [Z(x), H(t, x)]$  using the wet boundary condition (3.2.4) and the free surface boundary condition (3.2.5), we obtain:

$$\begin{aligned} \int_{Z(x)}^{H(t, x)} \text{RHS}(3.2.2) \, dz &= \left[ \frac{\mu_0}{\varepsilon} \partial_z u_\varepsilon \right]_{z=H(t, x)} - \left[ \frac{\mu_0}{\varepsilon} \partial_z u_\varepsilon \right]_{z=Z(x)} \\ &= - \left( k_+(R) + k_-(I) + k_0 \left( \frac{q}{h} \right) \right) \frac{q}{h}, \end{aligned} \quad (3.3.5)$$

where the friction factors  $k_+(R)$ ,  $k_-(I)$ , and  $k_0$  are defined by formulas (3.1.22) and (3.1.18), respectively. Finally, multiplying both sides of each of (3.3.3), (3.3.4), and

(3.3.5) by  $\rho_0 U^2/D$ , and recalling the mass-balance (3.3.3), we obtain the following *Saint-Venant system with recharge*:

$$\begin{aligned} \partial_t h + \partial_x q &= S := R - I, \\ \partial_t q + \partial_x \left[ \frac{q^2}{h} + g \frac{h^2}{2} \right] &= -g h \partial_x Z + S \frac{q}{h} - \left( k_+(R) + k_-(I) + k_0 \left( \frac{q}{h} \right) \right) \frac{q}{h} \quad (3.3.6) \\ &\text{where } q = hu, \end{aligned}$$

which we study in the rest of this paper.

**3.4. Example (lake at rest and filling the lake).** The still water steady state (also known as *lake at rest*) reads

$$q \equiv u \equiv S \equiv 0 \text{ and } h + Z \equiv H_0 \text{ for some constant } H_0 > 0. \quad (3.4.1)$$

This is a classical example used in testing the conservation properties of numerical schemes. Note that an interesting nontrivial example for numerical tests is  $S = R - I \equiv 0$  with  $R = I > 0$ .

Another simple (yet important) example is a space-time uniform filling of a lake with initial height  $h(0, \cdot) \equiv H_0$  as in (3.4.1) with a constant time-space  $S > 0$  and a spatially constant momentum with periodic boundary conditions. In this case, symmetry implies that system (3.3.6) simplifies to

$$\partial_t h \equiv S \text{ and } \partial_t q \equiv S \frac{q}{h} - \left( k_+(R) + k_-(I) + k_0 \left( \frac{q}{h} \right) \right) \frac{q}{h}, \quad (3.4.2)$$

with given initial conditions.

**3.5. Mixing friction.** In adapting the boundary conditions of the Navier-Stokes equations in §2.2 and §2.3, we included additional terms  $k_+(R)$  and  $k_-(I)$  that model the friction effect that occurs when water that is falling on the free surface or recharging through the ground, respectively, connects with the flow. The inclusion of these terms avoids certain paradoxical outcomes, such as perpetual motion, that otherwise occur when the terms are omitted. Such terms arise naturally from microscopic effects and have been discussed in the hydrology literature, for instance, by Wenzel [1970], Yoon and Wenzel [1971], Shen and Li [1973], Lu et al. [1998] where the laws are empirically derived from measurements. While the friction can be quite complex in behaviour depending on many of the involved quantities, but they share the characteristics of being monotone, zero at zero, and possibly homogeneous in the velocity  $u$  and the rates of additional water  $R$  and  $I$ , we consider the simplest such behaviour by taking.

To see the influence of the friction effect  $\alpha$  on the solution, we consider an idealised scenario that will enable us to calculate an *exact solution* to system (3.3.6). We take a constant rainfall–runoff process on a river spanning spatial domain  $x \in [0, 10]$  and time domain  $t \in [0, 1]$ , with topography  $Z \equiv 0.1$ ; for simplicity, we assume the infiltration  $I \equiv 0$  and a linear recharge friction  $k_+(R) = \alpha R$ . We prescribe periodic boundary conditions and assume a constant initial height and discharge of

$$h(0, x) = q(0, x) = 1 \text{ for } 0 < x < 10. \quad (3.5.1)$$

The rainfall intensity is applied uniformly on the river as a function of time up to the final time  $T = 1$ :

$$R(t) = 1.0 \text{ for } 0 < t < 1. \quad (3.5.2)$$

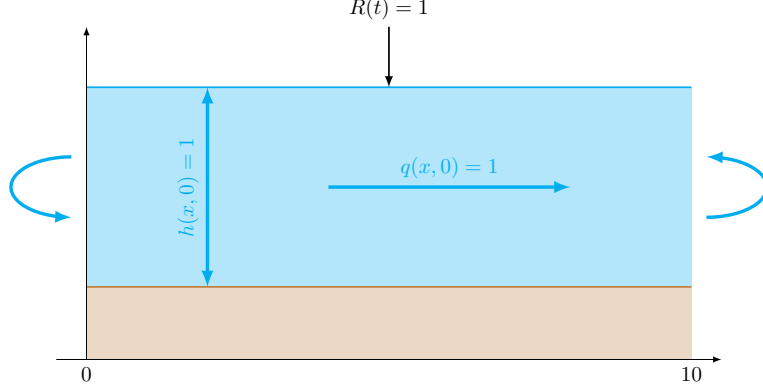


FIGURE 2. Diagram of the idealised scenario we are considering.

Since the rain function, initial height, and initial discharge do not have any dependence on  $x$ , we can ignore the spatial derivatives in both the mass and momentum equations. Under these assumptions, (3.3.6) simplifies to:

$$\begin{aligned} \partial_t h &= 1, \\ \partial_t q &= (1 - \alpha) \frac{q}{h} \quad \text{where } q = hu. \end{aligned} \quad (3.5.3)$$

We can solve explicitly for  $h$  and  $q$  (which are constant in space) and the corresponding velocity

$$h(t, x) = t + 1, \quad q(t, x) = (t + 1)^{1-\alpha}, \quad u(t, x) = (t + 1)^{-\alpha}. \quad (3.5.4)$$

Using these equations, we can plot how the *momentum* and *velocity* change over time depending on the mixing friction coefficient  $\alpha$ . We consider three cases, reported in Figure 3,

- $\alpha < 1$  water entering the course produces too little friction to slow the flow down. In this regime, the velocity remains constant or decreases over time while the *momentum increases* at the rate of increase in water height. The exclusion, or weakness, of the additional friction terms  $k_-(I)$  and  $k_+(R)$  leads to a paradox, as momentum is being produced even though the rain is assumed to fall with zero momentum. We can conclude, therefore, that this regime leads to an unrealistic physical system.
- $\alpha = 1$  the friction generated by the rain causes a reduction in velocity that balances the increase in height. We are thus in the situation where the additional terms in the conservation of momentum equation cancel one another out. In this regime, momentum is conserved over time due to the balance between the increase in momentum from the  $Ru$  term and the reduction in momentum from the additional friction term; this leads to a reduction in velocity over time. As the momentum is conserved within the system, this regime is physically realistic.
- $\alpha > 1$  the friction generated by the rain exceeds the increase in momentum from the  $Ru$  term. We are thus in the situation where the additional friction term is dominant. In this regime, the additional friction term slows the flow at a faster rate than the increase in water height; therefore, momentum and velocity both decrease over time. The reduction in momentum due to the higher friction effect means the regime is physically realistic.

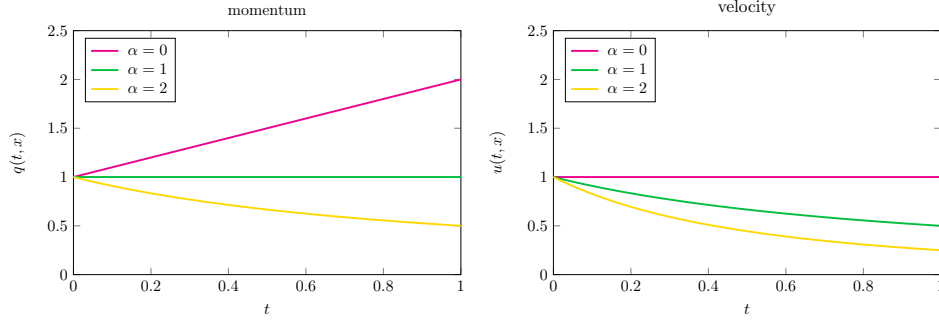


FIGURE 3. Exact solution's momentum and velocity in three cases of mixing friction coefficient  $\alpha$  as discussed in § 3.5. The case  $\alpha = 0$  means no mixing friction whatsoever and leads to a *physical paradox* where momentum increases in time as mass increases. The case  $\alpha = 1$  is critical and ensures no artificial momentum gain, but this case is also an unrealistic idealised situation because it implies momentum conservation in presence of mixing friction. Finally the case  $\alpha > 1$  is the most physically relevant.

We can conclude from considering this idealised scenario that the additional friction terms cannot be omitted, as doing so leads to a paradoxical situation where the momentum increases over time even though the rain is assumed to be added to the system with zero momentum. We therefore only have physically realistic solutions when the friction  $\alpha \geq 1$ , as it is within this regime that the momentum is either conserved or decreasing. As is clear from the equations, this occurs when the reduction in velocity is large enough to either compensate or balance the increase in water height.

#### 4. ENTROPY

Entropy plays an essential role in the analytical and numerical understanding of conservation and balance laws [Evans, 2013, Serre, 1999, Dafermos, 2010]. In this section we study the effect of the rainfall terms and associated mixing friction on the entropy–entropy-flux pair, for the Saint-Venant system (3.3.6), in particular the effect of the additional rainfall terms have on entropy production.

**4.1. Theorem (hyperbolicity and stability of (3.3.6)).** *Let  $(h, q)$  with satisfy the Saint-Venant system with recharge (3.3.6) for a given topography  $Z$ , rainfall  $R$  and infiltration  $I$ , with velocity*

$$u := \frac{q}{h} \quad (4.1.1)$$

and total head  $\psi := \hat{\psi}(h, q, Z)$  defined by

$$\hat{\psi}(h, q, Z) := \frac{q^2}{2h^2} + g(h + Z), \text{ for } (h, q, Z) \in \mathbb{R}^+ \times \mathbb{R}^2. \quad (4.1.2)$$

Then the following hold:

- (a) System (3.3.6) is strictly hyperbolic on the set  $\{h > 0\}$ .
- (b) If  $(h, q)$  is smooth and  $h > 0$ , we have the velocity balance equation

$$\partial_t u + \partial_x \psi = -\frac{(k_+(R) + k_-(I) + k_0(u))u}{h}. \quad (4.1.3)$$

*Proof.* The proof follows standard arguments from conservation laws and is provided for self-containment's sake. We consider each statement in turn.

(a) The Jacobian of (3.3.6)'s *flux function*  $(q, h) \mapsto (q, q^2/h + g h^2/2)$  is given by

$$\mathbf{J} = \hat{\mathbf{J}}(h, q) := \begin{bmatrix} 0 & 1 \\ -q^2/h^2 + g h & 2q/h \end{bmatrix}, \quad (4.1.4)$$

with eigenvalues

$$\lambda_{1,2} = \hat{\lambda}_{1,2}(h, q) = \frac{q}{h} \pm \sqrt{g h}. \quad (4.1.5)$$

For these eigenvalues to be real and distinct, we require that  $h > 0$ ; the Jacobian matrix is thus diagonalizable and system (3.3.6) is strictly hyperbolic on the set  $\{h > 0\}$ .

(b) We rewrite the conservation of momentum equation in system (3.3.6) in terms of the unknowns  $(h, u)$ , with  $u = q/h$ , as

$$\partial_t [hu] + \partial_x \left[ hu^2 + g \frac{h^2}{2} \right] = -g h \partial_x Z + Su - (k_+(R) + k_-(I) + k_0(u)) u. \quad (4.1.6)$$

Applying the product rule to the first term of (4.1.6) and substituting in the conservation of mass equation, we get

$$\begin{aligned} h \partial_t u + u (S - \partial_x [hu]) + \partial_x [hu^2] + \partial_x \left[ g \frac{h^2}{2} \right] \\ = -g h \partial_x Z + Su - (k_+(R) + k_-(I) + k_0(u)) u, \end{aligned} \quad (4.1.7)$$

from which we can cancel  $Su$  on both sides. Using the product rule again, we have that

$$u \partial_x [hu] = \partial_x [hu^2] - hu \partial_x u, \quad (4.1.8)$$

which can be substituted into (4.1.7) to give

$$\begin{aligned} h \partial_t u - \partial_x [hu^2] + hu \partial_x u + \partial_x [hu^2] + \partial_x \left[ g \frac{h^2}{2} \right] \\ = -g h \partial_x Z - (k_+(R) + k_-(I) + k_0(u)) u, \end{aligned} \quad (4.1.9)$$

enabling us to now cancel  $\partial_x [hu^2]$ . We note that

$$\partial_x \left[ g \frac{h^2}{2} \right] = h \partial_x [g h]. \quad (4.1.10)$$

Substituting this into (4.1.9) and dividing by  $h$  throughout, we get

$$\partial_t u + u \partial_x u + \partial_x [g h] = -g \partial_x Z - \frac{(k_+(R) + k_-(I) + k_0(u)) u}{h}. \quad (4.1.11)$$

Making the further substitution

$$u \partial_x u = \partial_x [u^2]/2 \quad (4.1.12)$$

and grouping derivatives of  $x$ , we have

$$\partial_t u + \partial_x \psi = -\frac{(k_+(R) + k_-(I) + k_0(u)) u}{h} \quad (4.1.13)$$

as required.

The theorem is thus proven.  $\square$

**4.2. Remark (friction effects).** It is worth noting that the only way  $S = R - I$  enters in the velocity balance equation (4.1.3) is through the friction terms  $k_+(R)$  and  $k_-(I)$ . This is a further indication that these terms are necessary, especially for small water height  $h$ , which as a denominator of the right-hand side in (4.1.3) amplifies the effects of friction as these occur in the Navier–Stokes on a layer close to the boundaries.

**4.3. Theorem (entropy production).** Consider the entropy and entropy flux respectively defined by

$$\hat{E}(h, q, Z) := \frac{q^2}{2h} + g h \left( \frac{h}{2} + Z \right) = \frac{hu^2 + g h^2}{2} + g h Z, \quad (4.3.1)$$

$$\hat{\Psi}(h, q, Z, S) := \left( \hat{E}(h, q) + \frac{g h^2}{2} \right) \frac{q}{h} - g \Theta. \quad (4.3.2)$$

where

$$\Theta(t, x) := \int_0^x S(t, s) Z(s) \, ds \text{ for each } t > 0, x \in \mathbb{R} \quad (4.3.3)$$

The pair of functions  $(\hat{E}, \hat{\Psi})$  forms a mathematical entropy–entropy-flux pair for system (3.3.6) when  $S \equiv 0$  and  $k_i = 0$  for  $i = 0, \pm$ . Furthermore for smooth solutions  $(h, q)$  of (3.3.6), the functions

$$E := \hat{E}(h, q, Z) \text{ and } \Psi := \hat{\Psi}(h, q, Z, S) \quad (4.3.4)$$

satisfy the following entropy production relation

$$\partial_t E + \partial_x \Psi = S \left( \frac{u^2}{2} + g h \right) - (k_+(R) + k_-(I) + k_0(u)) u^2. \quad (4.3.5)$$

**4.4. Remark (entropy–entropy-flux pairs and entropy production).** The entropy–entropy-flux pair of Theorem 4.3 is typical for shallow water equations [Audusse et al., 2000, Th. 2.1, e.g.]. Indeed (4.3.5), when  $S = 0$  and  $k_i = 0$ , for  $i = 0, \pm$ , generalises the well-known (zero) *entropy condition*

$$\partial_t E + \partial_x \Psi = 0, \quad (4.4.1)$$

which implies that  $(\hat{E}, \hat{\Psi})$  is an entropy–entropy-flux pair. The additional term  $-g\Theta$  in (4.3.2) corresponds to the flux of entropy due to the added or subtracted rain; thanks to this term the entropy production is frame invariant.

**4.5. Proof of Theorem 4.3.** In view of 4.4 it is enough to prove only (4.3.5). We begin by recalling that we showed in Theorem 4.1(b) that the conservation of momentum equation can be rewritten in terms of the velocity  $u$  as

$$\partial_t u + \partial_x \psi = - \frac{(k_+(R) + k_-(I) + k_0(u)) u}{h}, \quad (4.5.1)$$

where  $\psi$  is the total head, given by

$$\psi = \frac{u^2}{2} + g h + g Z. \quad (4.5.2)$$

Proceeding from this, multiplying the conservation of mass equation by  $\psi$  we have

$$\psi \partial_t h + \psi \partial_x [hu] = S \psi \quad (4.5.3)$$

which we can rewrite as

$$\partial_t [\psi h] + \partial_x [\psi hu] - (h \partial_t \psi + (hu) \partial_x \psi) = S \psi. \quad (4.5.4)$$

The term  $h\partial_t\psi$  in the second component can be expanded as

$$\begin{aligned} h\partial_t\psi &= \frac{h}{2}\partial_t[u^2] + hg\partial_t h + hg\partial_t Z \\ &= (hu)\partial_t u + \frac{g}{2}\partial_t[h^2]. \end{aligned} \quad (4.5.5)$$

In the second component we may write

$$\partial_x\psi = -\partial_t u - \frac{(k_+(R) + k_-(I) + k_0(u))u}{h} \quad (4.5.6)$$

from (4.5.1), and hence, after cancelling terms, we have

$$\partial_t[\psi h] + \partial_x[\psi hu] - \left( \partial_t \left[ g \frac{h^2}{2} \right] + (k_+(R) + k_-(I) + k_0(u))u^2 \right) = S\psi, \quad (4.5.7)$$

which can be rewritten as

$$\partial_t \left[ \psi h - g \frac{h^2}{2} \right] + \partial_x[\psi hu] = S\psi - (k_+(R) + k_-(I) + k_0(u))u^2. \quad (4.5.8)$$

Expliciting  $\psi$  as a function of  $h, q, S, Z$  and noting that

$$\partial_x \left[ g \int_0^x S(s, t) Z(s) ds \right] = g S(t, x) Z(x) \text{ for each } (t, x) \quad (4.5.9)$$

concludes the proof.  $\square$

**4.6. Remark (discontinuous solutions).** In Theorems 4.1 and 4.3, we only made reference to smooth solutions  $(h, u)$  in defining the stability and entropy relations of the Saint-Venant system (3.3.6). For rough weak solutions, as with conservation laws, the entropy-entropy-flux pair  $(\hat{E}, \hat{\Psi})$  has the potential to play a selection mechanism role to ensure uniqueness of weak solutions as it does with conservation laws.

## 5. THE NUMERICAL MODEL

We now consider the numerical approximation of the Saint-Venant system with rain. We follow the approach developed by Audusse et al. [2000], Perthame and Simeoni [2001], with a suitable modification to accommodate the additional source and friction terms. While any well-balanced computational finite volume method could be adapted to simulate our model [Kröner, 1997, LeVeque, 1992, 2002, Toro, 2009, Bouchut, 2004, Kurganov, 2018], the kinetic approach has the pleasant feature of naturally including the additional term  $Su$ , and thereby also the corresponding friction coefficients  $k_+(R)$  and  $k_-(I)$ , in the Saint-Venant system. As a result, as observed in Audusse et al. [2000] the resulting schemes are automatically up-winded and well balanced.

**5.1. Well balanced schemes.** A desirable property of the standard Saint-Venant system is the preservation of equilibrium states (referred to as the *lake-at-rest*), given by

$$h + Z = \text{constant} \text{ and } u = 0. \quad (5.1.1)$$

For our system, since through the addition of rainfall and infiltration effects we no longer have a conservation law but rather a balance law, we have the possibility of water being added to or lost from the lake, and thus this particular equilibrium only holds in the case  $S = 0$ . We must adapt this property therefore, and instead desire that our system preserves the *filling-the-lake* state (see Figure 4), given by

$$\partial_t h = R \text{ and } u = 0, \quad (5.1.2)$$



that is, the rate at which the water height changes is equal to the rate at which water is added to the system through the rainfall term. Failing to preserve this property would mean a change in the mass of the water that is greater or lower than the rate at which it is added, thus violating the balance of mass property of our system.

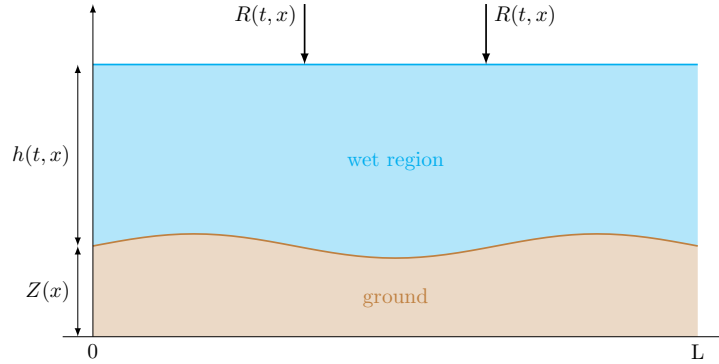


FIGURE 4. In considering a balance law system, we must adapt the *lake-at-rest* property used for conservation laws to account for the addition of water.

If we wish to maintain this property, we cannot rely on the usual finite difference or finite volume methods, and thus a new (so called well-balanced) scheme is required. Such an approach can be found by going back to a kinetic interpretation of the system, as detailed in Perthame and Simeoni [2001] and Ersoy [2015]. The method we use for the derivation of our kinetic scheme will follow much the same approach, though with the added complication of accounting for the additional terms. These *kinetic solvers* can be modified to preserve the filling-the-lake state, while at the same time maintaining their simplicity and stability properties.

One of the direct benefits of using such an approach for the Saint-Venant system is the ability of the kinetic solver to deal with dry soil cases (that is, when  $h = 0$ ) Audusse et al. [2000], which will be of importance in ensuring our model continues to function if infiltration causes the water level to fall close to zero, or if we consider cases such as water flowing away from a beach front.

**5.2. Kinetic function.** To derive the kinetic equation for system (3.3.6), we follow the kinetic formulation proposed by Audusse et al. [2000], Perthame and Simeoni [2001] and further developed by Bourdarias et al. [2014], Ersoy [2015]. We consider a *kinetic averaging weight function*  $\chi : \mathbb{R} \rightarrow \mathbb{R}$  and a *kinetic density function*  $M$  satisfying

$$\chi(\omega) = \chi(-\omega) \geq 0, \quad \int \chi(\omega) \, d\omega = 1, \quad \int \omega^2 \chi(\omega) \, d\omega = \frac{g}{2}, \quad (5.2.1)$$

$$M(t, x, \xi) := \sqrt{h(t, x)} \chi\left(\frac{\xi - u(t, x)}{\sqrt{h(t, x)}}\right). \quad (5.2.2)$$

These functions originate in the kinetic theory where  $M(t, x, \xi)$  accounts for the density of particles with speed  $\xi$  at the space-time point  $(t, x)$ .

In developing a numerical method, the goal is for the derivation of the finite-volume scheme fluxes to be based on  $M$ , through the following property which links the macroscopic variables with the microscopic ones.

**5.3. Proposition (macroscopic-microscopic relations).** *Let the functions  $h, u$  solve the Saint-Venant system (3.3.6) and  $M$  as in (5.2.2). If  $h(t, x) > 0$  at  $(t, x)$  then the following macroscopic-microscopic relations hold*

$$\int_{\mathbb{R}} \begin{bmatrix} 1 \\ \xi \\ \xi^2 \end{bmatrix} M(t, x, \xi) \, d\xi = \begin{bmatrix} h(t, x) \\ h(t, x)u(t, x) \\ h(t, x)u(t, x)^2 + gh(t, x)^2/2 \end{bmatrix}. \quad (5.3.1)$$

Recalling our Saint-Venant system (3.3.6), we note that, by substituting  $u = q/h$  (for  $h > 0$ ), the topography and friction terms on the right-hand side of the conservation of momentum equation can be rewritten as

$$-gh\partial_x Z - (k_+(R) + k_-(I) + k_0(u))u = -gh \left( \partial_x Z + \frac{(k_+(R) + k_-(I) + k_0(u))u}{gh} \right), \quad (5.3.2)$$

following the approach considered in, for example, Bourdarias et al. [2011], adapted to account for our additional friction terms. The reason for rewriting these terms in this manner is so we can pack them into a single divergence form; that is, we define the *nonlinear flux integral operator*

$$\hat{W}[h(t, \cdot), u(t, \cdot)](x) := Z(x) + \int_0^x \left[ \frac{(k_+(R) + k_-(I) + k_0(u))u}{gh} \right](t, s) \, ds \quad (5.3.3)$$

for each  $x \in \mathbb{R}$ , and system (3.3.6) thus becomes

$$\begin{aligned} \partial_t h + \partial_x [hu] &= S \\ \partial_t [hu] + \partial_x \left[ hu^2 + \frac{gh^2}{2} \right] &= -gh\partial_x \hat{W}[h, u] + Su. \end{aligned} \quad (5.3.4)$$

The kinetic scheme approach allows us to connect the Saint-Venant system with the single scalar equation obtained by introducing an auxiliary *microscopic velocity* variable  $\xi$  and looking at the evolution of the density  $(0, T) \times \mathbb{R}^2 \ni (t, x, \xi) \mapsto M(t, x, \xi)$  as the solution of the following semilinear *kinetic equation*

$$\partial_t M + \xi \partial_x M - g \partial_x \hat{W} \left[ \langle M \rangle_0, \frac{\langle M \rangle_1}{\langle M \rangle_0} \right] \partial_\xi M + \frac{SM}{\langle M \rangle_0} = Q, \quad (5.3.5)$$

where we use the following *moment* notation for  $m = 0, 1, \dots$

$$\langle M \rangle_m := \int_{\mathbb{R}} \xi^m M(\cdot, \cdot, \xi) \, d\xi. \quad (5.3.6)$$

The right-hand side in (5.3.5),  $Q(t, x, \xi)$ , plays the mathematical role of a *collision term*, similar, for instance, to the ones encountered in Boltzmann's equation. In view of Proposition 5.3, if  $(h, u)$  satisfying (3.3.6) is given, the pair  $(M, Q)$  defined by (5.2.2) and (5.3.5) satisfy the collision 0-moment condition

$$\langle Q \rangle_m = 0 \text{ for } m = 0, 1. \quad (5.3.7)$$

Conversely, each pair of functions  $(M, Q)$  satisfying (5.3.5) and (5.3.7) provides a pair  $(h, u)$  satisfying (3.3.6) by taking

$$h := \langle M \rangle_0 \text{ and } hu := \langle M \rangle_1. \quad (5.3.8)$$

We take a second here to note why the additional notation for  $\langle M \rangle_0$  and  $\langle M \rangle_1$  is required. In defining  $\hat{W}$ , we assume that  $(h, u)$  are unknown and to be found, and thus we cannot use them within the definition. We are required, therefore, to instead define  $\hat{W}$  in terms of  $\langle M \rangle_0$  and  $\langle M \rangle_1$ , which are themselves defined in terms of the density function  $M$ , the solution to the kinetic equation, and which by virtue of the macroscopic-microscopic relations (5.3.1) will ultimately give us  $h$  and  $u$ .

**5.4. Remark (advantages of the kinetic formulation).** While the kinetic approach is one of many possibilities, and not without drawbacks, we mention some of its nice features:

- (i) In contrast to previous work, e.g., Perthame and Simeoni [2001], the kinetic equation (5.3.5) contains an extra term accounting for precipitation and infiltration effects. This departure is crucial for the derivation of the fluxes that lead to a well-balanced scheme in the presence of such terms.
- (ii) We also note that, even though the Maxwellian  $M$  is constructed for still water steady states, where  $S(t, x) = 0$ , we can still use it here to ensure a well-balanced scheme.
- (iii) In general, it is easier to find a numerical scheme to solve equation (5.3.5) for  $M$  that has the properties we desire, such as entropy stability, than to solve the full Saint-Venant system for  $h$  and  $u$ . However, in finding  $M$ , we can calculate  $h$  and  $hu$  by virtue of the macro-microscopic relations (proposition 5.3). In fact,  $M$  is never calculated explicitly, rather the function

$$\hat{M}(\zeta, \varphi) := \sqrt{\zeta} \chi \left( \frac{\varphi}{\sqrt{\zeta}} \right) \quad (5.4.1)$$

$$\text{whereby } M(t, x, \xi) = \hat{M}(h(t, x), \xi - u(t, x)),$$

is used to build the fluxes appearing in a finite volume method, as we shall explain in §5.5.

**5.5. Discretisation and kinetic fluxes.** To go from the kinetic equation (5.3.5) to a numerical method, we follow the approach of Perthame and Simeoni [2001], in which they developed a kinetic scheme for the standard Saint-Venant system, i.e. equation (5.3.5) with  $S = 0$ . Their approach was based on the general method for developing a finite volume scheme, integrating the kinetic equation over the domain of interest, with the vector of unknowns defined as

$$U_i^n = \int_{\mathbb{R}} \begin{bmatrix} 1 \\ \xi \end{bmatrix} M_i^n(\xi) d\xi = \begin{bmatrix} h_i^n \\ h_i^n u_i^n \end{bmatrix}, \quad (5.5.1)$$

where the final equality can be seen from the macroscopic-microscopic relations (5.3.1) and in view of the second observation above. We follow the same process for our Saint-Venant system, giving us the numerical scheme

$$U_i^{n+1} = U_i^n - \frac{\Delta t}{\Delta x} \left( F_{i+1/2}^n - F_{i-1/2}^n \right) + \Delta t \begin{bmatrix} S_i^n \\ S_i^n u_i^n \end{bmatrix}, \quad (5.5.2)$$

where  $S_i^n$  is a discretisation of the combined rain and infiltration terms. We pick the time-step,  $\Delta t$ , according to

$$\Delta t = \frac{\text{CFL } \Delta x}{\max_i (|u_i^n| + \sqrt{2g h_i^n})}, \quad (5.5.3)$$

where  $\text{CFL} \in (0, 1]$  is the Courant–Friedrichs–Levy stability constant [Perthame and Simeoni, 2001, e.g.].

The construction of the numerical fluxes  $F_{i\pm 1/2}^n$  in (5.5.2) is based on the operator associated with  $\hat{M}$  given in (5.4.1). We give here a brief overview of how the successive numerical flux terms are developed; the interested reader is directed to Perthame and Simeoni [2001] and Bourdarias et al. [2014] for more details.

We define the numerical flux (which has two components representing the conservation of mass and momentum equations), as the integral

$$F_{i\pm\frac{1}{2}}^n := \int_{\mathbb{R}} \xi \begin{bmatrix} 1 \\ \xi \end{bmatrix} M_{i\pm\frac{1}{2}}^{\mp}(\xi) d\xi. \quad (5.5.4)$$

The intermediate quantities  $M_{i\pm\frac{1}{2}}^{\mp}(\xi)$ , which measure the flux at the upper and lower boundaries of the cell  $c_i = [x_{i-1/2}, x_{i+1/2}]$ , respectively, are realised as up-winded fluxes:

$$\begin{aligned} M_{i+1/2}^- &:= M_i^n(\xi) \mathbb{1}_{[\xi > 0]} + M_{i+1/2}^n(\xi) \mathbb{1}_{[\xi < 0]}, \\ M_{i-1/2}^+ &:= M_i^n(\xi) \mathbb{1}_{[\xi < 0]} + M_{i-1/2}^n(\xi) \mathbb{1}_{[\xi > 0]}, \end{aligned} \quad (5.5.5)$$

with

$$\begin{aligned} M_{i\pm\frac{1}{2}}^n &:= M_i^n(-\xi) \mathbb{1}_{[|\xi|^2 \leq 2g \Delta W_{i\pm\frac{1}{2}}^n]} \\ &+ M_{i\pm 1}^n \left( \mp \sqrt{|\xi|^2 - 2g \Delta W_{i\pm\frac{1}{2}}^n} \right) \mathbb{1}_{[|\xi|^2 \geq 2g \Delta W_{i\pm\frac{1}{2}}^n]}, \end{aligned} \quad (5.5.6)$$

where we use the notation

$$\mathbb{1}_{[P]} := \begin{cases} 1 & \text{if } P \text{ is true,} \\ 0 & \text{if } P \text{ is false.} \end{cases} \quad (5.5.7)$$

To understand how these fluxes are defined, consider the flux over the upper bound  $M_{i+1/2}^-$ . From (5.5.5), we can see that it comprises two terms:

- (i)  $M_i^n(\xi) \mathbb{1}_{[\xi > 0]}$ : movement of water with positive velocity ( $\xi > 0$ ) from within cell  $c_i$  to cell  $c_{i+1}$
- (ii)  $M_{i+1/2}^n(\xi) \mathbb{1}_{[\xi < 0]}$ : movement of water with negative velocity ( $\xi < 0$ ) from within cell  $c_{i+1}$  to cell  $c_i$ . This term is decomposed a second time into components reflecting whether the water has enough energy to overcome the topography and friction to enter or leave the cell.

A similar decomposition exists for the second term  $M_{i-1/2}^+$ , where this time we consider the negative and positive velocity of  $\xi$  for each case, respectively.

The term  $\Delta W_{i\pm\frac{1}{2}}^n$  is the upwinded source term and provides the jump condition necessary for a particle in one cell to overcome the friction and topography to move to an adjacent cell. Consistent with previous definitions, we calculate this term numerically as:

$$\Delta W_{i+1/2}^n = W_{i+1}(t_n) - W_i(t_n), \quad \Delta W_{i-1/2}^n = W_{i-1}(t_n) - W_i(t_n), \quad (5.5.8)$$

where

$$W_i(t) = \mathbb{1}_{[c_i]}(x) \frac{1}{\Delta x} \int_{c_i} W(t, x) dx \quad (5.5.9)$$

for a given cell  $c_i$ . The semi-discretised kinetic density,  $M_i^n$ , is defined as

$$M_i^n(\xi) := \sqrt{h_i^n} \chi \left( \frac{\xi - u_i^n}{\sqrt{h_i^n}} \right). \quad (5.5.10)$$

The discretisation we use in our scheme will be based upon the *Barrenblatt kinetic weighting function*

$$\chi(\omega) = \frac{1}{\pi g} \sqrt{(2g - \omega^2)_+} \quad \text{for } \omega \in \mathbb{R}, \quad (5.5.11)$$

where  $(X)_+$  stands for the positive part of  $X$  [Perthame and Simeoni, 2001, eq.(2.13)]. We note that this choice of function satisfies the properties we outlined in §5.2.

## 6. NUMERICAL TESTS

The kinetic scheme we use for our numerical method was implemented by extending the code of Besson et al. [2013] to account for the additional source term in (5.5.2), and we present here two simple numerical tests to demonstrate the validity and application of our Saint-Venant system and the associated numerical method. For this paper, we will focus on the rain term only and thus assume  $I \equiv 0$ ; the coupling of a realistic infiltration model with our Saint-Venant system and the treatment of the boundary conditions would be a paper in itself, and thus will be considered in future research.

In §6.1, we compare the accuracy of our numerical model to a flume experiment, considering how our results compare to both the physical data collected from this experiment and also previous numerical simulations of this experiment by other authors. Then, in §6.2, we simulate multiple rainfall processes of increasing duration on a slope with both a constant and decreasing gradient, and measure how the value of the friction effect  $\alpha$  impacts the solution.

**6.1. Comparison with real-world data.** For our first test, we explore the accuracy of our numerical scheme by comparing with data taken from the flume experiment run as part of the ANR project METHODE at INRA-Orléans; we also compare our results to those obtained by Delestre and James [2008], who considered only an addition to the conservation of mass equation.

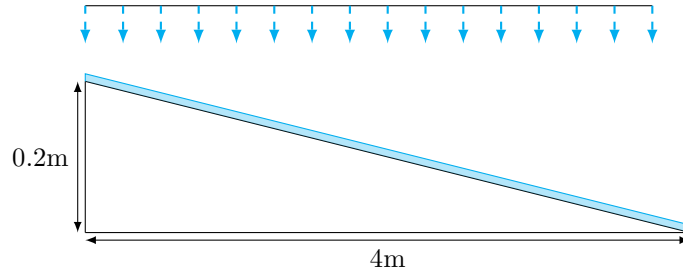


FIGURE 5. Visualisation of the flume experiment.

The experiment in question concerns a slope with a 5% gradient, an initial height  $h_0 = 0$ , and initial discharge  $q_0 = 0$ . The topography for the slope is given by

$$Z(x) = 0.2 - \frac{x}{20} \quad \forall x \in [0, 4], \quad (6.1.1)$$

we consider  $N = 1000$  meshpoints, and we assume a CFL number of 0.95. Rain falls onto the slope uniformly at a constant rate within a given time interval,

$$R(t, x) = \begin{cases} 50 \text{ mm/hr} & \text{if } (t, x) \in [5, 125] \times [0, 3.95], \\ 0 & \text{otherwise,} \end{cases} \quad (6.1.2)$$

and we measure the discharge at the downstream edge of the slope up to time  $T = 250$ s. For our simulation, we assume the rain-induced friction level  $\alpha = 1$ . The hydrograph for the experiment, together with the simulated values, is provided below in Figure 6.

The results from the simulation compare well with with the experimental data, particularly in the third and final phase when no rain is falling and the discharge is decreasing gradually over time. For the initial phase, where the discharge is

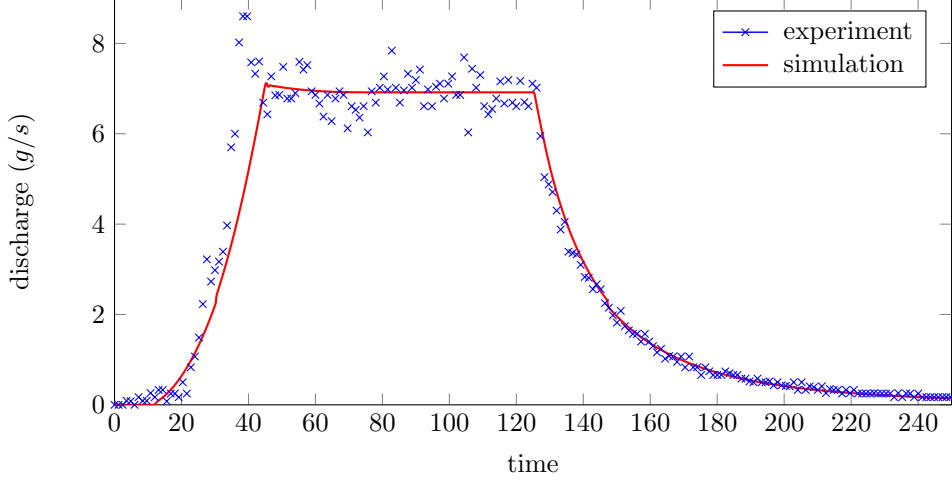


FIGURE 6. Hydrograph for the uniform slope test with both the experimental data and the simulated solution.

increasing, the simulation matches well to begin with (up to around 25s) but subsequently appears to increase at a slower rate than in the experiment; at  $t = 35$ s, for example, the experiment shows a discharge level of 5.7 g/s, compared to the simulation which is at 3.59 g/s. For the secondary phase, where the discharge has stabilised, while the simulation does not capture the fluctuations that were present in the experiment, it does maintain a smooth transition through the centre of the data, and begins to decrease at the same point as the experiment.

Comparing the results of our simulation to those of Delestre and James [2008], we see that our simulation matches much better in both the initial and final phases; in the initial phase, their simulation increases a lot sooner than in the experiment, and though it begins to decrease at the correct time, it also underestimates the total discharge level in the final phase. For the secondary phase, their results are slightly lower than ours but still consistent with the experimental data.

**6.2. Single-level and three-level cascade.** For our second test, we consider a similar scenario to §6.1 but with a higher intensity rainfall-runoff process on a slope with a much shallower gradient. We compare how the water flows when the gradient of the slope is constant, and how it flows when the gradient decreases periodically from the upstream to downstream end. We consider a spatial domain  $x \in [0, 12]$ , a final time  $t = 40$ s, a rainfall intensity  $R_0 = 0.001$  which falls across the entire domain,  $N = 1000$  meshpoints, and a CFL number of 0.95. The parameters that we want to change and measure the effect of are the following:

- (1) the total length of the rainfall process  $T_R = 10, 20,$  and  $30$  seconds
- (2) the topography of the slope onto which the rain falls, for which we consider a constant slope (the single cascade) with  $Z_1(x) = (12 - x)0.005$ , and a decreasing slope (the three-level cascade, see Figure 7) with

$$Z_2(x) = \begin{cases} (12 - x)0.006 - 0.012 & \text{if } x \in [0, 4] \\ (12 - x)0.005 - 0.004 & \text{if } x \in [4, 8] \\ (12 - x)0.004 & \text{if } x \in [8, 12] \end{cases} \quad (6.2.1)$$

- (3) the rain-induced friction level  $\alpha$ , for which we take  $\alpha = 0, 1$ , and  $5$  for the single cascade and  $\alpha = 0$  and  $1$  for the three-level cascade

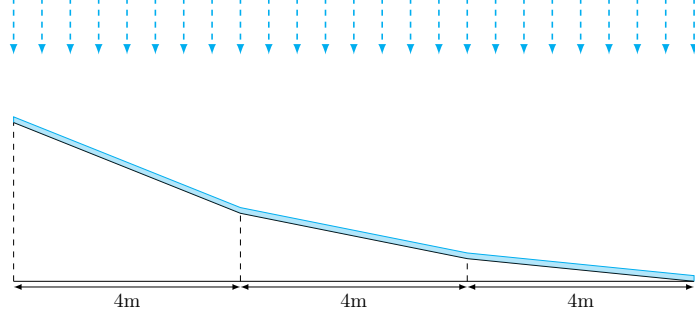


FIGURE 7. Topography for the three-level cascade, showing the decrease in gradient from the upstream to downstream end.

For our outputs, we measure the height of the flow across the entire domain at the point the rainfall stops, and we also measure the height and discharge at the downstream end (i.e.  $x = 12$ ) up to the final time.

Starting with the height profile at  $t = T_R$ , we see in Figure 8 that for the single-level cascade, increasing the value of  $\alpha$  causes more water to accumulate at the upstream end, as expected since the momentum of the water will decrease the higher the value of  $\alpha$ . It is interesting to note also that for  $T_R = 10$ , the water still accumulates to the same maximum amount irrespective of the value of  $\alpha$ , though at different points; for longer rainfall times, this accumulation can still occur, but potentially beyond the end of the domain if the water has enough momentum.

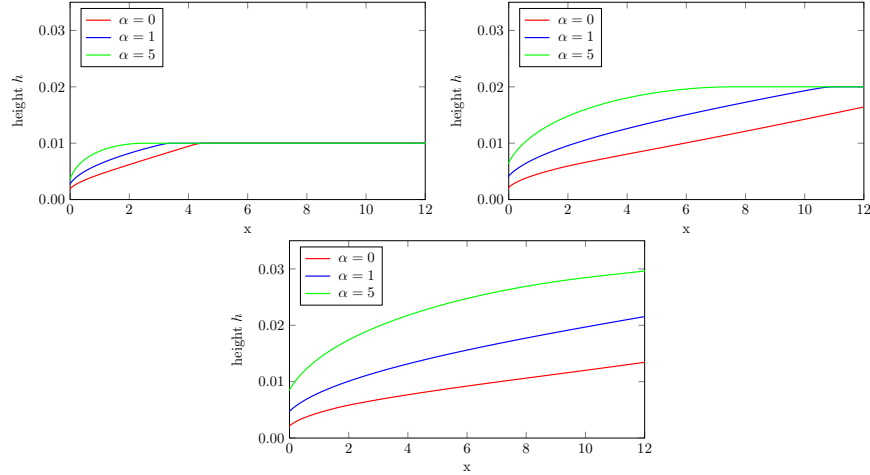


FIGURE 8. Height profiles for the single-level cascade for varying values of  $\alpha$  at the rainfall end time  $T_R = 10, 20$ , and  $30$ .

For the three-level cascade shown in Figure 9, the reduction in gradient induces multiple waves to be formed, though these waves become more smoothed out as the rainfall time increases. This effect is reduced as  $\alpha$  is increased, consistent with our expectation since the water flow will be more slowed. The flows do not accumulate to the same amount, though this may be due to the length of the domain.

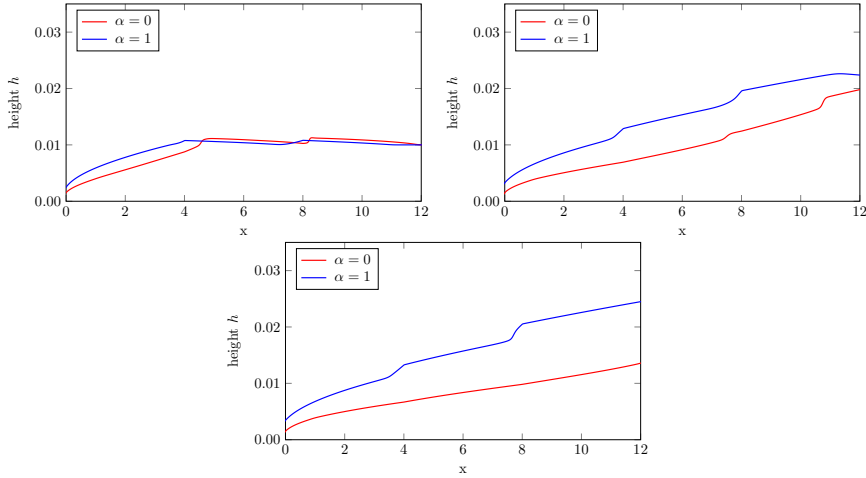


FIGURE 9. Height profiles for the three-level cascade for varying values of  $\alpha$  at the rainfall end time  $T_R = 10, 20,$  and  $30$ .

For the second part of our numerical test, we consider the height and momentum profiles over time at the end of the domain ( $x = 12$ ). For the single-level cascade (see Figure 10), we see that increasing the friction level  $\alpha$  extends the height profile of the flow, causing it to decrease at a later time. This occurs for all lengths of rainfall  $T_R$ , though notably we see that as  $T_R$  increases the length of time for which the flow plateaus is decreased.

For the momentum, the change in friction and length of rainfall has a much more pronounced effect. For  $T_R = 10$ , the three friction levels result in much the same profile though slightly shifted as the level increases. For  $T_R = 20$  and  $30$ , however, the profiles are more varied, with the momentum tending to change rather linearly for  $\alpha = 0$  but showing a much more curved profile for  $\alpha = 5$ . We can also see that for  $T_R = 30$ , the momentum is decreasing when the rainfall stops for  $\alpha = 0$  and  $1$ , but continues to rise and at an increased rate for  $\alpha = 5$ .

The three-level cascade shown in Figure 11 exhibits much the same behaviour as the single-level cascade, with perhaps the most notable changes being in the height profile; for the single-level cascade the height profile for  $\alpha = 0$  remains consistently below that for  $\alpha = 1$ , but for the three-level cascade this does not hold true between, approximately,  $t = 10$  and  $t = 20$ . The momentum profile for the three-level cascade is very similar in behaviour to the single-level.

## 7. CONCLUSION

Our aim in this paper was to derive a mathematically rigorous one-dimensional Saint-Venant system, extended to include both precipitation and infiltration effects. We achieved this by going back to the original two-dimensional Navier–Stokes equations and adapting the boundary conditions as appropriate to model these additional phenomena. The new model (3.3.6) that we have derived includes additional momentum source and friction terms in comparison to other models, which becomes special cases of our system. The friction terms are obtained naturally from the derivation and their presence is essential in explaining how the velocity of the water-body interacts with the additional water coming from either precipitation or runoff; we demonstrated in §3.5 that, for certain regimes, this model may



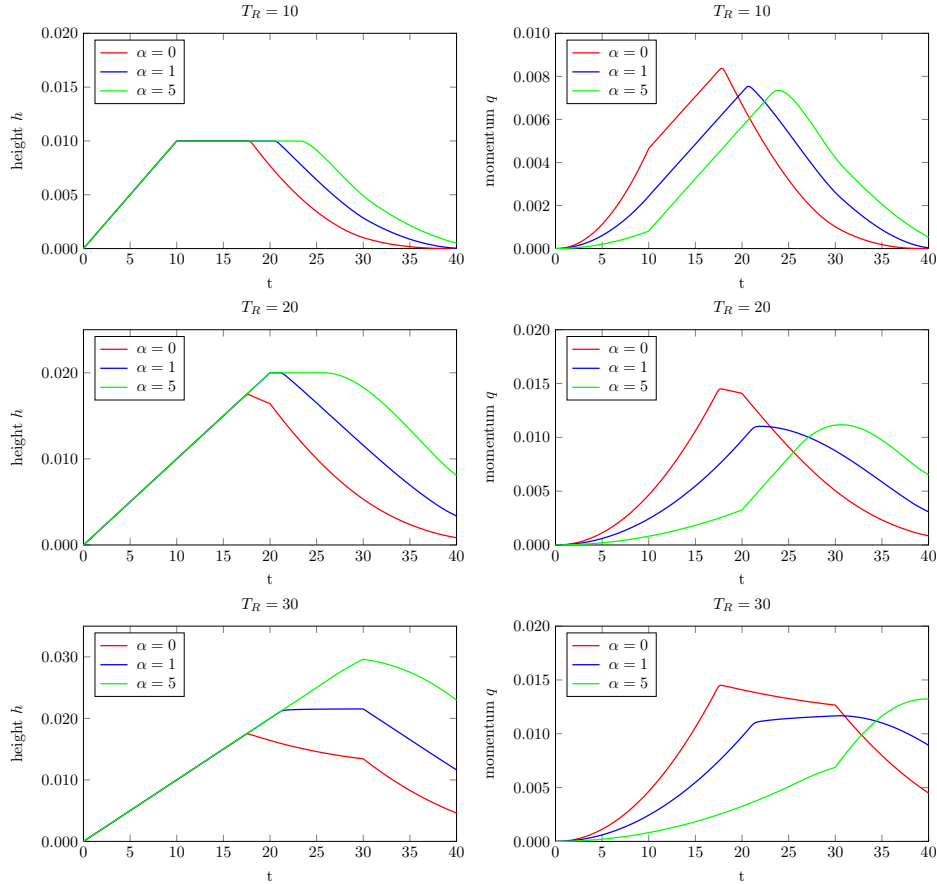


FIGURE 10. Height and momentum profiles over time for the single-level cascade for varying values of rain-induced friction  $\alpha$  at the domain end  $x = 12$ .

yield non-physical solutions. We showed in Theorem 4.1 that the existence of these additional terms leads to a model whose energetic consistency depends solely on the level of assumed rain-induced friction, denoted by  $\alpha$ .

In developing a numerical model, existing approaches such as finite difference or finite volume can be used, but they fail to ensure certain properties that we would like our method to have. The alternative approach we took was to instead use a kinetic formulation, writing our Saint-Venant system as a single kinetic equation which can then be solved using a finite volume method to find the original variables  $(h, q)$ . To demonstrate the applicability and viability of our system and associated kinetic scheme, we ran a number of numerical simulations of our model; in §6.1, we compared the accuracy of our model against a real-world experiment, while in §6.2 we saw that increasing the value of  $\alpha$  slows down the propagation of the flow; these results were all in line with our expectations and analysis of the model.

Though our Saint-Venant model goes some way to incorporating precipitation and infiltration effects, that it only includes one spatial dimension makes its application to modelling realistic real-world problems limited in scope, particularly on very large domains. The techniques and approach that we have used herein can be readily extended to the two-dimensional system, though some consideration needs

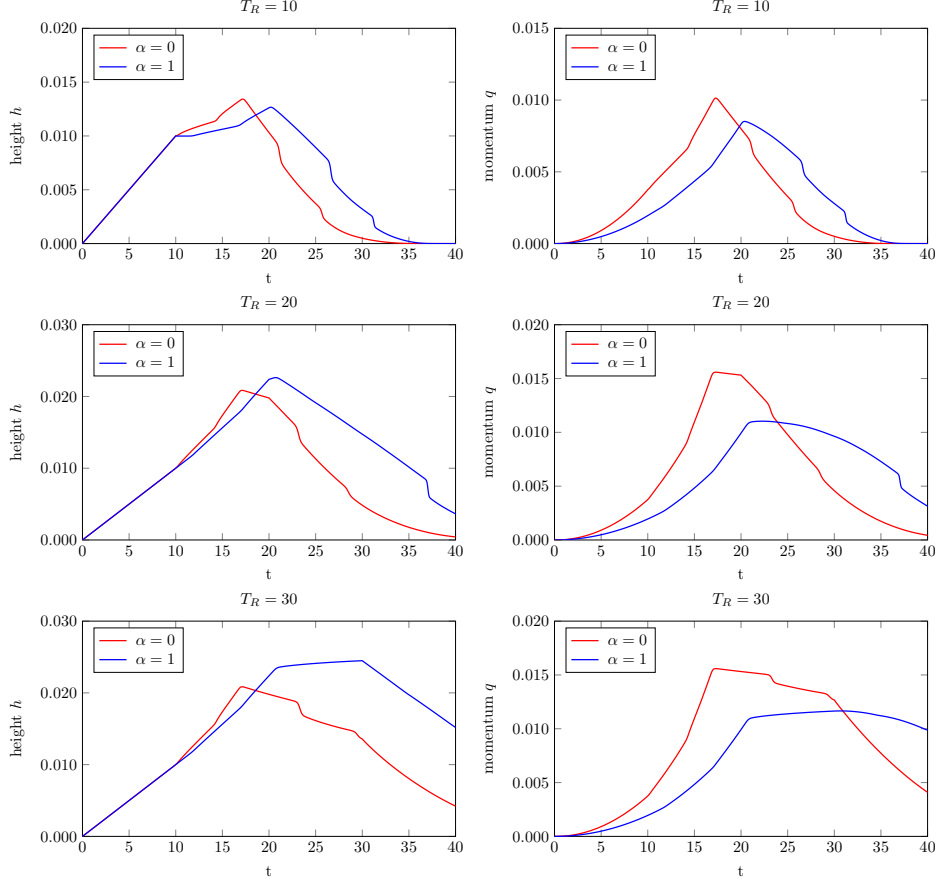


FIGURE 11. Height and momentum profiles over time for the three-level cascade for varying values of rain-induced friction  $\alpha$  at the domain end  $x = 12$ .

to be given to determine the friction terms and kinetic scheme for this system; we note, for example, that it is not clear the kinetic formulation we have derived for the one-dimensional model can be extended to a second dimension, and thus an entirely new approach may be required. This work is proposed for future research.

## 8. ACKNOWLEDGEMENTS

PT and OL were funded by the EPSRC (Engineering and Physical Sciences Research Council) via an EPSRC-CASE grant in collaboration with Ambiental Technical Solutions Ambiental.

OL would like to thank ME for the kind hospitality at the Université de Toulon in the framework of the “Professeur Invité” funding programme.

All authors acknowledge the support of the Marie Skłodowska-Curie ITN “Mod-CompShock” and the encouragement and useful remarks of Charalambos Makridakis, Martin Todd, Donatella Donatelli, Chiara Simeoni and Alexander Antonarakis.

## REFERENCES

- Ambiental. Ambiental environmental assessment a company of Royal Haskoning-DHV. URL <https://www.ambiental.co.uk>. pages 26
- E. Audusse, M.-O. Bristeau, and B. Perthame. Kinetic Schemes for Saint-Venant Equations with Source Terms on Unstructured Grids. Research Report RR-3989, INRIA, 2000. URL <https://hal.inria.fr/inria-00072657>. Projet M3N. pages 3, 15, 16, 17
- L. Badea, M. Discacciati, and A. Quarteroni. Numerical analysis of the Navier-Stokes/Darcy coupling. *Numerische Mathematik*, 115(2):195–227, 2010. ISSN 0029-599X. doi: 10.1007/s00211-009-0279-6. URL <https://doi.org/10.1007/s00211-009-0279-6>. pages 5
- G. S. Beavers and D. D. Joseph. Boundary conditions at a naturally permeable wall. *Journal of Fluid Mechanics*, 30(01):197–207, 10 1967. ISSN 1469-7645. doi: 10.1017/S0022112067001375. URL <https://doi.org/10.1017/S0022112067001375>. pages 5
- M. Besson, O. Lakkis, and P. Townsend. Finite volume code 1D Saint Venant. Sourceforge Library, 08 2013. URL <https://sourceforge.net/projects/finitevolumecode1dsaintvenant/>. pages 3, 21
- F. Bouchut. *Nonlinear Stability of Finite Volume Methods for Hyperbolic Conservation Laws: and Well-Balanced Schemes for Sources*. Frontiers in Mathematics. Birkhäuser Basel, 2004. ISBN 978-3-7643-6665-0. URL <https://www.springer.com/gp/book/9783764366650>. pages 16
- C. Bourdarias, M. Ersoy, and S. Gerbi. A kinetic scheme for transient mixed flows in non uniform closed pipes: a global manner to upwind all the source terms. *J. Sci. Comput.*, 48(1-3):89–104, 2011. ISSN 0885-7474. doi: 10.1007/s10915-010-9456-0. URL <https://dx.doi.org/10.1007/s10915-010-9456-0>. pages 18
- C. Bourdarias, M. Ersoy, and S. Gerbi. Unsteady mixed flows in non uniform closed water pipes: a full kinetic approach. *Numerische Mathematik*, 128(2): 217–263, 10 2014. ISSN 0945-3245. doi: 10.1007/s00211-014-0611-7. URL <https://doi.org/10.1007/s00211-014-0611-7>. pages 17, 19
- C. M. Dafermos. *Hyperbolic conservation laws in continuum physics*, volume 325 of *Grundlehren der Mathematischen Wissenschaften [Fundamental Principles of Mathematical Sciences]*. Springer-Verlag, Berlin, third edition, 2010. ISBN 978-3-642-04047-4. pages 13
- A.-J.-C. B. de Saint-Venant. Théorie du mouvement non-permanent des eaux, avec application aux crues des rivières at à l’introduction des marées dans leur lit. *Comptes rendus hebdomadaires des séances de l’Académie des sciences*, 73:147–154, 1871. URL <http://catalogue.bnf.fr/ark:/12148/cb343481087>. pages 2
- O. Delestre and F. James. Simulation of rainfall events and overland flow. In *X International Conference Zaragoza-Pau on Applied Mathematics and Statistics*, volume 35 of *Monografias del Seminario Matematico Garcia de Galdeano*, pages 125–135, Spain, Sept. 2008. Jaca. URL <https://hal.archives-ouvertes.fr/hal-00426694/document>. pages 21, 22

- O. Delestre, S. Cordier, F. Darboux, and F. James. A limitation of the hydrostatic reconstruction technique for Shallow Water equations. *Comptes Rendus Mathematique*, 350(13):677–681, July 2012. ISSN 1631-073X. doi: 10.1016/j.crma.2012.08.004. URL <https://arxiv.org/abs/1206.4986>. pages 2
- M. Ersoy. Dimension reduction for incompressible pipe and open channel flow including friction. In J. Brandts, S. Korotov, M. Křížek, K. Segeth, J. Šístek, and T. Vejchodský, editors, *Proceedings of the international conference Applications of Mathematics 2015, in honor of the birthday anniversaries of Ivo Babuška (90) and Milan Práger (85) and Emil Vitásek(85)*, pages 17–33, Prague, Czechia, Nov. 2015. Czech Academy of Sciences. ISBN 978-80-85823-65-3. URL <https://hal.archives-ouvertes.fr/hal-00908961v2>. to appear on Proceedings of the International Conference “Application of Mathematics 2015”, Prague. pages 6, 17
- M. Esteves, X. Faucher, S. Galle, and M. Vauclin. Overland flow and infiltration modelling for small plots during unsteady rain: numerical results versus observed values. *Journal of Hydrology*, 228(3):265–282, Mar. 2000. ISSN 0022-1694. doi: 10.1016/S0022-1694(00)00155-4. URL <http://www.sciencedirect.com/science/article/pii/S0022169400001554>. pages 2
- L. C. Evans. Entropy and partial differential equations. online lecture notes, Department of Mathematics, UC Berkeley, 2013. pages 13
- J.-F. Gerbeau and B. Perthame. Derivation of viscous Saint-Venant system for laminar shallow water; numerical validation. *Discrete and Continuous Dynamical Systems. Series B.*, 1(1):89–102, 2001. ISSN 1531-3492. doi: 10.3934/dcdsb.2001.1.89. URL <https://doi.org/10.3934/dcdsb.2001.1.89>. pages 5, 6
- R. Grace and P. S. Eagleson. Modeling of Overland Flow. *Water Resources Research*, 2(3):393–403, Sep 1966. ISSN 0043-1397. doi: 10.1029/WR002i003p00393. URL <http://doi.org/10.1029/WR002i003p00393>. WOS:A19668152300006. pages 2
- W. Jäger and A. Mikelić. On the interface boundary condition of Beavers, Joseph, and Saffman. *SIAM J. Appl. Math.*, 60(4):1111–1127 (electronic), 2000. ISSN 0036-1399. doi: 10.1137/S003613999833678X. URL <http://dx.doi.org/10.1137/S003613999833678X>. pages 5
- D. Kröner. *Numerical schemes for conservation laws*. Wiley-Teubner Series Advances in Numerical Mathematics. John Wiley & Sons, Ltd., Chichester; B. G. Teubner, Stuttgart, 1997. ISBN 0-471-96793-9. URL <http://www.worldcat.org/title/numerical-schemes-for-conservation-laws/oclc/36659525>. pages 16
- A. Kurganov. Finite-volume schemes for shallow-water equations. *Acta Numerica*, 27(Vol. 27 – 2018):289 – 351, May 2018. ISSN 0962-4929. doi: 10.1017/S0962492918000028. URL <http://browzine.com/articles/203182748>. Saved from BrowZine: <http://thirdiron.com/download>. pages 16
- R. J. LeVeque. *Numerical methods for conservation laws*. Lectures in Mathematics ETH Zürich. Birkhäuser Verlag, Basel, second edition, 1992. ISBN 3-7643-2723-5. doi: 10.1007/978-3-0348-8629-1. URL <http://dx.doi.org/10.1007/978-3-0348-8629-1>. pages 16

- R. J. LeVeque. *Finite volume methods for hyperbolic problems*. Cambridge Texts in Applied Mathematics. Cambridge University Press, Cambridge, 2002. ISBN 0-521-81087-6; 0-521-00924-3. doi: 10.1017/CBO9780511791253. URL <http://dx.doi.org/10.1017/CBO9780511791253>. pages 16
- C. D. Levermore and M. Sammartino. A shallow water model with eddy viscosity for basins with varying bottom topography. *Nonlinearity*, 14(6): 1493, 2001. ISSN 0951-7715. doi: 10.1088/0951-7715/14/6/305. URL <http://dx.doi.org/10.1088/0951-7715/14/6/305>. pages 5
- J.-Y. Lu, J.-Y. Chen, F.-H. Chang, and T.-F. Lu. Characteristics of shallow rain-impacted flow over smooth bed. *Journal of Hydraulic Engineering*, 124(12): 1242–1252, Dec. 1998. doi: 10.1061/(ASCE)0733-9429(1998)124:12(1242). URL [https://ascelibrary.org/doi/abs/10.1061/\(ASCE\)0733-9429\(1998\)124:12\(1242\)](https://ascelibrary.org/doi/abs/10.1061/(ASCE)0733-9429(1998)124:12(1242)). pages 11
- F. Marche. Derivation of a new two-dimensional viscous shallow water model with varying topography, bottom friction and capillary effects. *Eur. J. Mech. B Fluids*, 26(1):49–63, 2007. ISSN 0997-7546. doi: 10.1016/j.euromechflu.2006.04.007. URL <http://dx.doi.org/10.1016/j.euromechflu.2006.04.007>. pages 5
- B. Perthame and C. Simeoni. A kinetic scheme for the Saint-Venant system with a source term. *Calcolo*, 38(4):201–231, 2001. ISSN 0008-0624. doi: 10.1007/s10092-001-8181-3. URL <https://doi.org/10.1007/s10092-001-8181-3>. pages 3, 16, 17, 19, 20
- M. Rousseau, O. Cerdan, A. Ern, O. Le Maître, and P. Sochala. Study of overland flow with uncertain infiltration using stochastic tools. *Advances in Water Resources*, 38:1–12, 03 2012. ISSN 0309-1708. doi: 10.1016/j.advwatres.2011.12.004. URL <https://doi.org/10.1016/j.advwatres.2011.12.004>. pages 2
- P. G. Saffman. On the Boundary Condition at the Surface of a Porous Medium. *Studies in Applied Mathematics*, 50(2):93–101, June 1971. ISSN 1467-9590. doi: 10.1002/sapm197150293. URL <https://doi.org/10.1002/sapm197150293>. pages 5
- D. Serre. *Systems of Conservation Laws 1: Hyperbolicity, Entropies, Shock Waves*. Cambridge University Press, 05 1999. ISBN 978-1-139-42541-4. URL <http://www.worldcat.org/oclc/437072430>. pages 13
- H. W. Shen and R. Li. Rainfall effect on sheet flow over smooth surface. *Journal of the Hydraulics Division*, 99(hy5), 05 1973. URL <https://trid.trb.org/view/103314>. pages 11
- P. Sochala. *Numerical methods for subsurface flows and coupling with surface runoff*. phdthesis, Ecole des Ponts ParisTech, Dec. 2008. URL <https://hal.archives-ouvertes.fr/pastel-00004625>. pages 2
- V. L. Streeter, E. B. Wylie, and K. W. Bedford. *Fluid mechanics*. WCB/McGraw Hill, Boston, 1998. ISBN 978-0-07-062537-2 978-0-07-115600-4. URL <http://www.worldcat.org/oclc/37475163>. OCLC: 37475163. pages 5
- E. F. Toro. *Riemann solvers and numerical methods for fluid dynamics*. Springer-Verlag, Berlin, third edition, 2009. ISBN 978-3-540-25202-3. doi: 10.1007/b79761. URL <http://www.worldcat.org/oclc/609677474>. A practical introduction. pages 16

- S. Weill, E. Mouche, and J. Patin. A generalized Richards equation for surface/subsurface flow modelling. *Journal of Hydrology*, 366(1–4):9–20, Mar. 2009. ISSN 0022-1694. doi: 10.1016/j.jhydrol.2008.12.007. URL <https://doi.org/10.1016/j.jhydrol.2008.12.007>. pages 2
- H. G. J. Wenzel. The effect of raindrop impact and surface roughness on sheet flow. Research Report 34, Water Rresearch Centre University of Illinois, 09 1970. URL <https://core.ac.uk/display/158313273?recSetID=>. FINAL REPORT Project No. B-018-ILL. pages 2, 11
- D. A. Woolhiser and J. A. Liggett. Unsteady, one-dimensional flow over a plane—The rising hydrograph. *Water Resources Research*, 3(3):753–771, 1967. ISSN 0043-1397. doi: 10.1029/WR003i003p00753. URL <https://doi.org/10.1029/WR003i003p00753>. pages 2
- E. B. Wylie and V. L. Streeter. *Fluid transients*. McGraw-Hill International Book Co., New York, 1978. URL <http://adsabs.harvard.edu/abs/1978mhi..book.....W>. pages 5
- Y. N. Yoon and H. G. Wenzel. Mechanics of sheet flow under simulated rainfall. *Journal of the Hydraulics Division*, 11 1971. URL <https://trid.trb.org/view/103996>. pages 11
- W. Zhang and T. W. Cundy. Modeling of two-dimensional overland flow. *Water Resources Research*, 25(9):2019–2035, 09 1989. ISSN 1944-7973. doi: 10.1029/WR025i009p02019. URL <https://doi.org/10.1029/WR025i009p02019>. pages 2

MEHMET ERSOY  
UNIVERSITÉ DE TOULON, IMATH EA 2134, LA GARDE (FRANCE), FR-83957

*E-mail address:* Mehmet.Ersoy@univ-tln.fr

*URL:* <http://ersoy.univ-tln.fr/>

OMAR LAKKIS  
DEPARTMENT OF MATHEMATICS, UNIVERSITY OF SUSSEX, BRIGHTON (ENGLAND, UNITED KINGDOM), GB-BN1 9QH

*E-mail address:* lakkis.o.maths@gmail.com

PHILIP TOWNSEND  
CHALMERS UNIVERSITY OF TECHNOLOGY, CHALMERSPLATSEN 4, 412 96 GOTHENBURG (SWEDEN)

*E-mail address:* phil.townsend123@gmail.com